THE FLAMMABILITY OF ELECTRONIC COMPONENTS IN SPACECRAFT ENVIRONMENTS

By Sami Atallah, Ulrich Bonne and John N. de Ris

October 1968

Prepared under Contract No. NAS 12-623 by
FACTORY MUTUAL RESEARCH CORPORATION
Norwood, Massachusetts

Electronics Research Center

NATIONAL AERONAUTICS AND SPACE ADMINISTRATION

Mr. Irving Litant
Technical Monitor
NAS 12-623
Electronics Research Center
National Aeronautics and Space Administration
575 Technology Square
Cambridge, Massachusetts 02139

Requests for copies of this report should
be referred to:

NASA Scientific and Technical Information Facility
P. O. Box 33
College Park, Maryland 20740

THE FLAMMABILITY OF ELECTRONIC COMPONENTS IN SPACECRAFT ENVIRONMENTS

By Sami Atallah, Ulrich Bonne and John N. de Ris

October 1968

Prepared under Contract No. NAS 12-623 by
FACTORY MUTUAL RESEARCH CORPORATION
Norwood, Massachusetts

Electronics Research Center

NATIONAL AERONAUTICS AND SPACE ADMINISTRATION

FOREWORD

The studies described in this report were performed during the period 15 March - 15 October 1968 on NASA Contract NAS 12-623 at the Factory Mutual Research Corporation. Three scientific papers are in preparation at this time. Abstracts of two papers have been submitted for presentation at the 1969 meeting of the Central States Section - The Combustion Institute to be held March 18-19, 1969 in Minneapolis, Minnesota:

(i) U. Bonne: "Radiative Extinction of Diffusion Flames"

(ii) S. Atallah, U. Bonne and J. N. deRis "Fires in Spacecraft Environments"

The third paper will cover the theoretical aspects of zero-gravity combustion and is being prepared by J. N. deRis.

ACKNOWLEDGEMENTS

The authors wish to acknowledge the constructive comments and suggestions made by Mr. C. Yao of FMRC. They also would like to thank their colleagues S. N. Bajpai and J. S. Kim for performing the more tedious calculations. Messrs. R. W. Crandlemere and K. Harvey helped in the performance of the experimental studies.

ABSTRACT

A theorectical model was presented to describe combustion in a zero gravitational field. The differential equations describing energy and mass conservation of such a system were solved by assuming:

1. Very fast reaction rates.
2. Stoichiometric combustion at the reaction zone.
3. Radiative heat losses proportional to the rate of heat release by combustion.
4. Flat fuel surface.

Expressions were derived for the burning rate of the fuel, the flame temperature and position and other combustion parameters. A criterion for the flammability of a fuel in a zero-g field was also derived. The implications of this model were discussed.

An upper limit for flame extinguishment time was found by calculating the time necessary for a laminar diffusion flame to cool below the ignition temperature by radiation only. A flat diffusion flame burner was constructed and used to estimate the extinguishment time. Satisfactory agreement was obtained when compared with the extinguishment time for paraffin as found in experiments performed in aircraft traversing zero-g curves. Other methods for simulating zero-g in the laboratory were suggested.

Equations predicting the temperature and pressure rise due to a fast developing fire in an enclosure were derived. Several models for the burning of solid materials were postulated and used to predict temperature and pressure variation with time. The results were compared with experimental data and with the Apollo accident pressure record. Both sources indicate that a burning model leading to an exponential increase of burning rate with time is the most appropriate.

Previous work on the self-heating of wire bundles was reviewed. The derivations were extended to the case of a sheathed wire bundle. Recommendations for further work on bundles consisting of different wires carrying varying loads were made.

TABLE OF CONTENTS

LIST OF FIGURES

NOMENCLATURE

A	Surface area (cm^2)
B	Mass transfer driving "force" = $\frac{Y_{o\infty}\ Q\ (1-\chi)}{M_o\ \nu_o'\ L} - \frac{Cp\ (Tvap-T_\infty)}{L}$
C_p	Specific heat (cal/g^oC)
$\bar{C}_p$	Average molar specific heat (Cal/g-mole ^oC)
c	Number of carbon atoms in $C_c\ H_h\ O_x$
D	Mass diffusivity (cm^2/s)
d	Diameter (cm)
f_v	Volumetric fraction occupied by soot (dimensionless)
H	Heat of combustion (cal/g)
h	Heat transfer coefficient (cal/cm^2s ^oK) Number of hydrogen atoms in $C_c\ H_h\ O_x$
k	Overall thermal conductivity of wire bundle (cal/ cm s ^oK) Fuel evaporation constant (cm^2/s) constant
L	Heat of vaporization (cal/g) Hot gas layer or flame thickness (cm)
Le	Lewis Number = $\frac{\lambda}{\rho C_p D}$ (dimensionless
M	Molecular weight (g/mole)
m	Mass of fuel (g)
$\dot{m}$	Mass burning rate (g/s)
$\dot{m}_i''$	Rate of specie "i" mass generation per unit area (g/s cm^2)
$\dot{m}_i'''$	Rate of specie "i" mass generation per unit volume (g/s cm^3)
N	Number of moles
n	$(\rho v)_{y=o}\ \frac{1}{\rho_\infty}\ \sqrt{\frac{t}{D_\infty}}$ (dimensionless)
P	Pressure (atm)
Q	Heat liberated by burning ν_F' moles of fuel (cal) Heat content of enclosure (cal)
$\dot{q}'''_{chem}$	Rate of heat generation per unit volume (cal/s cm^3)

Nomenclature (Cont'd)

$\dot{q}'''_{rad}$	Rate of radiation emitted by flame per unit volume (cal/s cm^3)
q'''	Rate of energy developed per unit volume
R	Gas constant (atm cm^3/g-mole ^oK)
$R_1(t)$	Radiative heat transfer received by fuel surface (cal/cm^2s)
r_1	$\frac{2\ R_1(t)}{L\ \rho_\infty}\ \sqrt{\frac{t}{D_\infty}}$ (dimensionless)
s	Radius of wire bundle (cm)
T	Temperature (^oK)
t	Time (s)
V	Volume of enclosure (cm^3)
v	Velocity of gas away from vaporizing surface (cm/s)
x	Number of oxygen atoms in $C_c\ H_h\ O_x$
X	Characteristic diffusion length (cm)
Y	Mass fraction in the vapor phase (dimensionless)
y	Distance away from the fuel bed (cm)
z	Height (cm)

Greek Letters

α	Proportionality constant
β	$\frac{q_o \alpha}{k_1}$
ϵ	emissivity (dimensionless)
ς	$\frac{\lambda_\infty\ y}{2\lambda_w\ \sqrt{D_\infty\ t}}$ (dimensionless)
θ	$T-T_o$ (^oK)
λ	Thermal conductivity (cal/cm s ^oK)
	also $\frac{h_c + h_r}{k}$ (cm^{-1})
ν_i', ν_i''	Stoichiometric coefficients (mol)

Nomenclature (Cont'd)

ξ $\quad \dfrac{1}{2\sqrt{D_\infty t}} \int_0^y \dfrac{\rho}{\rho_\infty}\, dy$ (dimensionless)

ρ Density (g/cm^3)

σ Stefan - Boltzmann constant
$= 1.355\ (10^{-12})$ cal s^{-1} cm^{-2} $^oK^{-4}$

τ Time (s)
Transmissivity (dimensionless)
Thickness (cm)

Φ_1 $\quad \dfrac{C_p(T-T_\infty)}{L} + \dfrac{(Y_O-Y_{O\infty})\ Q\ (1-\chi)}{M_O\ \nu_O'\ L}$ (dimensionless)

Φ_2 $\quad \dfrac{Y_F\ Q\ (1-\chi)}{M_F\ \nu_F'\ L} - \dfrac{(Y_O-Y_{O\infty})\ Q\ (1-\chi)}{M_O\ \nu_O'\ L}$ (dimensionless)

Φ_3 $\quad \dfrac{C_p\ (T-T_\infty)}{L}$ (dimensionless)

χ Fraction of chemical energy released in the form of radiation.

Subscripts

F	Fuel
f	Flame
g	Gas
o	Oxygen, initial
P	Product
s	Soot
w	Fuel bed
∞	Ambient
1	Initial, also wire bundle
2	Final, also sheath

1. INTRODUCTION

The use of high oxygen concentrations in manned spacecraft coupled with physical restrictions on the movement and egress of occupants present a fire hazard unlike any encountered normally on Earth. In addition, the behavior of fires under an abnormal gravitational field is not completely understood. This is particularly true during weightlessness the duration of which is usually the longest period in current spaceflights.

Since it is impossible to remove non-flammable materials from the space cabin completely (food, human hair and skin are combustible) one can only try to reduce these combustibles to a minimum. Furthermore, one cannot completely eliminate thermal energy sources. The need for electric energy to power communication, refrigeration and other devices presents the other link needed to initiate the combustion process.

The main purpose of this study was to consider combustion in zero gravity theoretically and to attempt to simulate its essential features in the laboratory. In addition, the temperature and pressure rise due to a fire in an enclosure and the self-heating of electric wire bundles were to be investigated.

2. COMBUSTION AT ZERO-G

2.1 Influence of Gravitational Forces on Fires

A space vehicle experiences short durations of high-g forces during launch and re-entry. An orbiting vehicle is essentially at zero-g, while a vehicle on the lunar surface experiences one-sixth of the gravitational force present on Earth. In studying fire hazards within space vehicles, the role that gravitational forces play in the combustion processes have to be considered. The rate of burning and the composition of combustion products are governed to a large extent by the rate at which these products are removed from the burning surface. This rate, in turn, is dependent on buoyant forces which result from density differences in the gravitational field.

In comparison with work on flammability in oxygen enriched atmospheres, combustion under a gravitational force other than that on Earth, has received very little attention. The reason for this is that it is rather difficult and inconvenient to reproduce high, low or zero-g in the laboratory. High-g can be generated in a centrifuge but the apparatus must be large enough to contain the necessary instrumentation. Flammability experiments performed at Atlantic Research Corporation [1] in a centrifuge have shown that an increase in g increases the upward rate of fire spread on vertical surfaces of solid combustibles. This effect was most pronounced between one and six-g but not much beyond six-g. The average heat flux and heat transfer coefficient from the flame increased slowly. Theoretically, these should vary with $g^{0.25}$ for laminar flames and $g^{0.4}$ for turbulent flames. The temperature levels and profiles and the flame height were not significantly affected at high-g.

Low-g can be produced by allowing a mass to fall freely while connected to a smaller counterweight through a pulley system (Atwood machine). Again, the size of the apparatus must be large if long duration steady state observations are desired. Such an apparatus was used by Kumagai and Isoda [2,3] to study the burning rate of liquid fuel droplets at low-g. These results agree with what one would expect by extrapolating high-g data.

Zero-g experiments on Earth employing free fall [2,3] are again limited in duration by the height of fall (1 second for a 4.9m fall, 2 seconds for a 19.6m fall). Aircraft travelling in zero-g curves have been employed [4,5,6] to give between 12 and 28 seconds. These times are still too short to make such quantitative observations as the rate of burning, ignition and flame temperatures and the composition of combustion products. Consequently, zero-g tests have, thus far, been essentially limited to qualitative observations and photography. Ideal zero-g combustion experiments would require an orbiting satellite. A series of a hundred zero-g flammability tests is planned as one of the experiments to be performed on the Multi-Dock Adapter of the Orbital Workshop which is part of the Apollo Application Program [7].

Because of the difficulty and expense in performing true zero-g experiments and because of the lack of information in this area, an attempt has been made to simulate the essential phenomena occurring during zero-g combustion by theoretical and experimental models. These attempts are described in the following paragraphs.

2.2 Mathematical Model

2.2.1 Description of Simplified Model

Figure 1 shows a simplified theoretical model of combustion at zero-g. Because of the absence of convection, the flame moves away from the fuel and toward the oxygen. Meanwhile, the fuel bed absorbs heat as its temperature rises toward the vaporization temperature of the fuel, T_{vap}. The fuel bed receives energy from the flame and the hot combustion products by conduction and radiation. The excess energy which is not absorbed by the fuel bed serves to vaporize the fuel. The fuel vapor diffuses toward the flame front, where the fuel reacts with the available oxygen. The concentration of fuel and oxygen are zero at the flame. (This implies an infinitely fast reaction rate.)

As time increases, the flame moves further away from the fuel bed and the characteristic diffusion length for fuel and oxygen increases. Thus, the concentration and temperature gradients decrease and consequently, the combustion rate decreases.

2.2.2 Formulation of the Governing Differential Equations

Gas Phase

The single global reaction, taking place at the flame front is

$$\nu'_F \text{ (Fuel)} + \nu'_o \text{ (Oxygen)} \longrightarrow \nu''_{P_1} \text{ (Product \#1)} + \nu''_{P_2} \text{ (Product \#2)} + \text{Heat}$$

where ν'_i and ν''_i are the usual stoichiometric coefficients.

Define Q as the heat released by the combustion of ν'_F moles of fuel with ν'_o moles of oxygen.

It will be assumed that a constant fraction χ of the heat released by combustion will be in the form of radiation. The combustion of $M_F \nu'_F$ grams of fuel will thus result in χ Q radiative heat release.

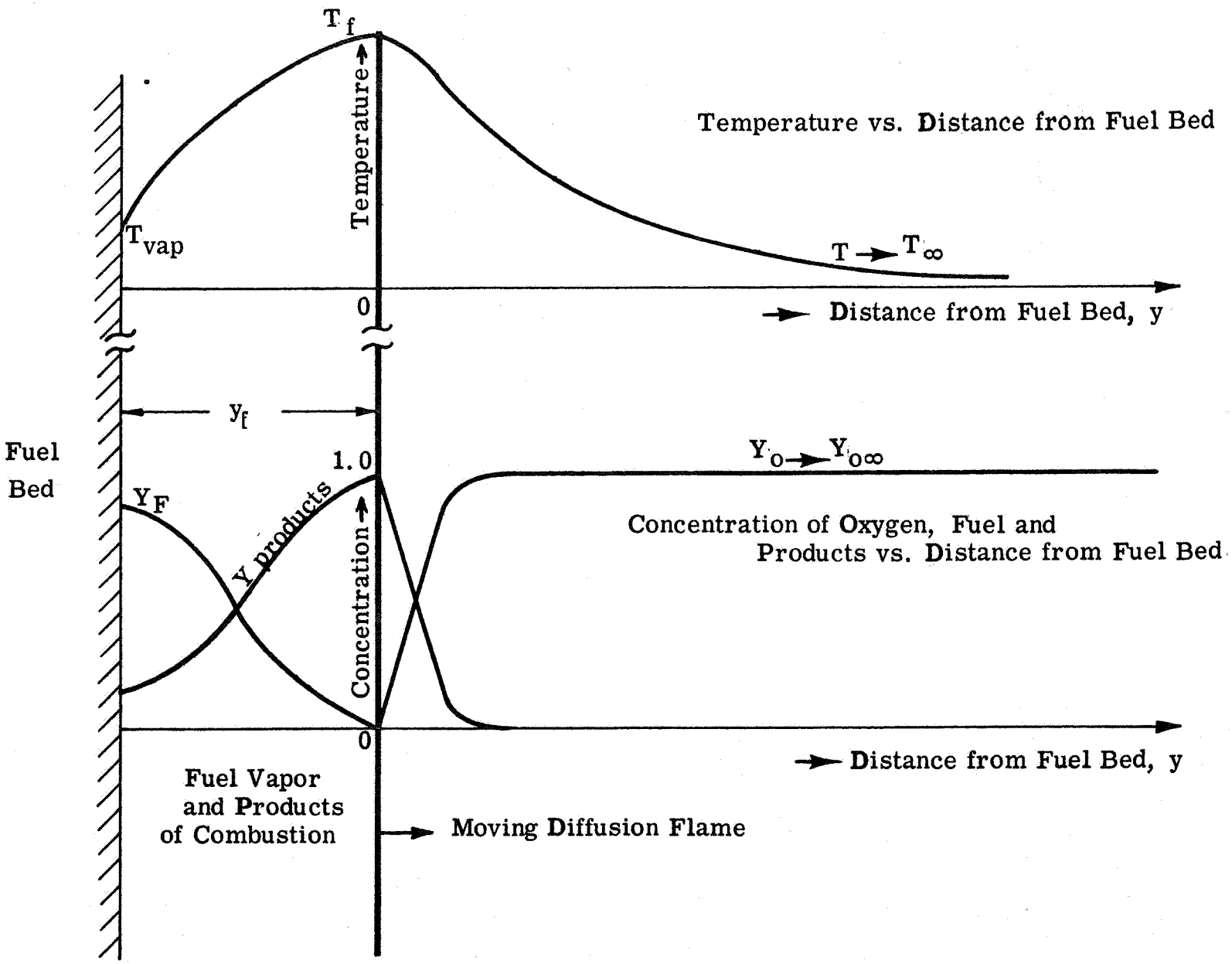

FIGURE 1. - THEORETICAL MODEL FOR ZERO-G COMBUSTION

If the gases are assumed transparent, and the fuel bed has an emissivity ϵ, then the radiant heat received by the fuel bed is $(1/2)\epsilon\chi Q$ for the combustion of $M_F \nu'_F$ grams of fuel. Only half of this radiation is directed toward the fuel bed.

A Lewis number, Le = $\lambda/(\rho C_p D)$, of unity is assumed, since the molecular processes of thermal diffusion and mass diffusion are similar.

The time-dependent one-dimensional thermal energy equation is

$$\rho C_p \frac{\partial T}{\partial t} + \rho C_p v \frac{\partial T}{\partial y} - \frac{\partial}{\partial y}\left(\lambda \frac{\partial T}{\partial y}\right) = \dot{q}'''_{chem} - \dot{q}'''_{rad} \qquad (1)$$

where $\dot{q}'''_{chem}$ is the rate of thermal energy released by combustion per unit volume, and $\dot{q}'''_{rad} = \chi \dot{q}'''_{chem}$ is the net rate of radiative heat loss per unit volume.*

The time-dependent one-dimensional specie equations are

$$\rho \frac{\partial Y_i}{\partial t} + \rho v \frac{\partial Y_i}{\partial y} - \frac{\partial}{\partial y}\left(\rho D \frac{\partial Y_i}{\partial y}\right) = \dot{m}'''_i \qquad (2)$$

where $Y_i(y,t)$ is the mass concentration of specie "i", and $\dot{m}'''_i$ is the mass rate of formation of specie "i" per unit volume.

Now consider the dimensionless function:

$$\varphi_1(y,t) = \frac{C_p(T - T_\infty)}{L} + \frac{(Y_O - Y_{O\infty})\, Q\,(1 - \chi)}{M_O \nu'_O\, L} \qquad (3)$$

where L is the heat of vaporization of the fuel, while T_∞ and $Y_{O\infty}$ are respectively the ambient temperature and oxygen concentration at

---

* Since convective heat losses due to density gradients are absent at zero-g the only energy loss mechanism, besides conduction is radiation. In order to facilitate the solution of the energy equation, the net radiative heat loss is approximated by $\dot{q}'''_{rad} = \chi \dot{q}'''_{chem}$.

infinity. For convenience φ_1 has been defined so as to be zero at infinity. By combining the energy equation and oxygen specie equation with unity Lewis number, one has

$$\rho \frac{\partial \varphi_1}{\partial t} + \rho v \frac{\partial \varphi_1}{\partial y} - \frac{\partial}{\partial y}\left(\frac{\lambda}{C_p} \frac{\partial \varphi_1}{\partial y}\right) = \frac{\dot{q}'''_{chem}\,(1-\chi)}{L} + \frac{\dot{m}'''_o\, Q\,(1-\chi)}{M_o\, \nu'_o\, L}$$

$$= 0 \qquad (4)$$

The right hand side of this equation is zero because the heat, $\frac{Q\,(1-\chi)}{M_o\,\nu'_o}$ is released into the temperature field when unit mass of oxygen is consumed.

Similarly, consider the dimensionless function

$$\varphi_2\,(y,t) = \frac{Y_F\, Q\,(1-\chi)}{M_F\,\nu'_F\, L} - \frac{(Y_o - Y_{o\infty})\, Q\,(1-\chi)}{M_o\,\nu'_o\, L} \qquad (5)$$

By combining the specie equations for fuel and oxygen, one has

$$\rho \frac{\partial \varphi_2}{\partial t} + \rho v \frac{\partial \varphi_2}{\partial y} - \frac{\partial}{\partial y}\left(\frac{\lambda}{C_p} \frac{\partial \varphi_2}{\partial y}\right) =$$

$$= \frac{\dot{m}'''_F\, Q\,(1-\chi)}{M_F\,\nu'_F\, L} - \frac{\dot{m}'''_o\, Q\,(1-\chi)}{M_o\,\nu'_o\, L} \qquad (6)$$

$$= 0$$

The right hand of this equation is also zero, because $M_F\,\nu'_F$ grams of fuel are consumed with $M_o\,\nu'_o$ grams of oxygen.

The continuity equation provides

$$\frac{\partial \rho}{\partial t} + \frac{\partial}{\partial y}(\rho v) = 0 \qquad (7)$$

Since the velocity, v, is always much less than the speed of sound, one can assume that the pressure is constant and ignore the momentum

equation. Assuming that the chemical reaction does not significantly increase the number of moles, the equation of state at a constant pressure provides

$$\rho T = \rho_\infty T_\infty \tag{8}$$

Fuel Bed

Assuming constant properties of the fuel bed, the conduction equation is

$$\rho_w C_{p_w} \frac{\partial T}{\partial t} + \rho_w C_{p_w} v_w \frac{\partial T}{\partial y} - \lambda_w \frac{\partial^2 T}{\partial y^2} = 0, \text{ for } y \leqslant 0 \tag{9}$$

where the convection (i.e. middle) term describes the slow motion of the fuel bed toward the stationary vaporizing fuel surface. This term is relatively negligible.

Conservation of mass at the fuel surface implies that

$$\rho_w v_w (t) = (\rho v)\Big|_{y=0}$$

Thus, in terms of the dimensionless temperature

$$\varphi_3 (y, t) = \frac{C_p (T - T_\infty)}{L}$$

The above fuel bed conduction equation becomes

$$\frac{\partial \varphi_3}{\partial t} + \frac{1}{\rho_w} (\rho v)\Big|_{y=o} \frac{\partial \varphi_3}{\partial y} - \frac{\lambda_w}{\rho_w C_{p_w}} \frac{\partial^2 \varphi_3}{\partial y^2} = 0 \tag{10}$$

Boundary Conditions

φ_1 and φ_2 are defined so that

$$\varphi_1 \text{ and } \varphi_2 \longrightarrow 0 \quad \text{as } y \longrightarrow \infty \quad \text{or } t \longrightarrow 0 \tag{11}$$

Also φ_3 is defined so that

$$\varphi_3 \longrightarrow 0 \text{ as } y \longrightarrow \infty \quad \text{or } t \longrightarrow 0 \tag{12}$$

At the vaporizing surface, the temperature of both the gas and the fuel bed will be quite close to the boiling point of the fuel, T_{vap}. Noting that there is no oxygen immediately above the fuel surface, one has

$$\varphi_3\,(0,t) = \frac{C_p\,(T_{vap} - T_\infty)}{L} \tag{13}$$

and

$$\varphi_1\,(0,t) = \frac{C_p\,(T_{vap} - T_\infty)}{L} - \frac{Y_{o\infty}\quad Q\,(1-\chi)}{M_o\ \nu'_o\ L} \tag{14}$$

$$= - B$$

where B is commonly called the mass transfer driving "force".

At the fuel bed surface the rate of fuel vaporization is proportional to the net heat transfer to the surface. If $(\rho v)_{y=o}$ is the mass flux from the surface

$$(\rho v)\Big|_{y=o} L = \lambda \frac{\partial T}{\partial y}\Big|_{y=o} + R_1\,(t) - \lambda_w \frac{\partial T}{\partial y}\Big|_{y=o}$$

where L is the heat of vaporization of the fuel (presumed constant), and R_1 (t) is the net radiant heat transfer received by the surface. In terms of φ_1 and φ_3, this equation becomes

$$(\rho v)_{y=o} = \frac{\lambda}{C_p} \frac{\partial \varphi_1}{\partial y}\Big|_{y=o+} + \frac{R_1(t)}{L} - \frac{\lambda_w}{C_p} \frac{\partial \varphi_3}{\partial y}\Big|_{y=o-} \tag{15}$$

The final fuel surface boundary condition describes how the fuel surface mass flux $(\rho v)_{y=o}$ is carried by bulk flow (convection) and diffusion into the gas phase. Thus

$$(\rho v)_{y=o} = (\rho v)_{y=o} Y_F (0,t) - \rho D \frac{\partial Y_F}{\partial y} (0,t)$$

or in terms of Φ_2

$$\rho D \frac{\partial \Phi_2}{\partial y}\bigg|_{y=o+} = - (\rho v)_{y=o} \left[\frac{Q (1 - \chi)}{M_F \nu'_F L} + \frac{Y_{o\infty} Q (1 - \chi)}{M_o \nu'_o L} - \Phi_2(0,t) \right] \quad (16)$$

Except for the specification of the radiative heat transfer term R_1 (t), the formulation is now complete. The five governing equations (4), (6), (7), (8), and (10), with the initial conditions (11) and (12), and the boundary conditions (11-16) form a well set problem for the five unknowns ρ, v, Φ_1, Φ_2 and Φ_3.

2.2.3 Solution

These equations and boundary conditions can be considerably simplified by the following similarity transformation which also transforms the temperature dependent density, conductivity and diffusivity to their ambient values.

Let

$$\xi = \frac{1}{2\sqrt{D_\infty t}} \int_o^y \frac{\rho}{\rho_\infty} dy, \quad \text{for } y \geqslant 0 \quad (17)$$

$$\xi = \frac{\lambda_\infty y}{2 \lambda_w \sqrt{D_\infty t}}, \quad \text{for } y \leqslant 0 \quad (18)$$

$$\tau = t \quad (19)$$

$$r_1(\tau) = \frac{2\, R_1(\tau)}{L\ \rho_\infty} \sqrt{\frac{\tau}{D_\infty}} \tag{20}$$

and

$$n(\tau) = \frac{1}{\rho_\infty} \sqrt{\frac{\tau}{D_\infty}}\ (\rho v)_{y=o} \tag{21}$$

The last equation defines the dimensionless mass transfer $n(\tau)$ which, together with $r_1(\tau)$, will be shown to be independent of τ.

Using equations (7), (17) and (19) one obtains

$$\left.\frac{\partial \xi}{\partial \tau}\right|_y = \frac{-\xi}{2\tau} - \frac{\rho\, v}{2\, \rho_\infty \sqrt{D_\infty \tau}} + \frac{n(\tau)}{2\,\tau}$$

and

$$\left.\frac{\partial \xi}{\partial y}\right|_\tau = \frac{\rho}{2\ \rho_\infty \sqrt{D_\infty\, \tau}}$$

Using the chain rule, the gas-phase equations (4) and (6) become

$$4\tau \frac{\partial \varphi_i}{\partial \tau} + 2\left\{n(\tau) - \xi\right\} \frac{\partial \varphi_i}{\partial \xi} - \frac{\partial^2 \varphi_i}{\partial \xi^2} = 0 \quad \text{for } i = 1,\ 2;\ \xi \geqslant 0 \tag{22}$$

where $\rho\lambda$ is assumed constant and equal to $\rho_\infty\, \lambda_\infty$. Again, a unit Lewis number, $\dfrac{\lambda_\infty}{\rho_\infty C_p D_\infty} = 1$ is assumed.

The fuel bed equation, (10), becomes

$$4\tau \frac{\partial \varphi_3}{\partial \tau} + 2\left\{\frac{\rho_\infty \lambda_\infty}{\rho_w\ \lambda_w}\, n(\tau) - \varsigma\right\} \frac{\partial \varphi_3}{\partial \varsigma} - \frac{\lambda_\infty\ \rho_\infty\ C_p}{\lambda_w\ \ \rho_w\ C_{p_w}} \frac{\partial^2 \varphi_3}{\partial \varsigma^2} = 0$$

$$\text{for } \varsigma \leqslant 0 \tag{23}$$

The initial conditions and boundary conditions (11 to 16) become respectively

$$\Phi_1 \text{ and } \Phi_2 \longrightarrow 0 \qquad \text{as } \xi \longrightarrow \infty \tag{24}$$

$$\Phi_3 \longrightarrow 0 \qquad \text{as } \zeta \longrightarrow -\infty \tag{25}$$

$$\Phi_3 \Big|_{\zeta=o} = \frac{C_p\,(T_{vap} - T_\infty)}{L} \tag{26}$$

$$\Phi_1 \Big|_{\xi=o} = -B \tag{27}$$

$$2\,n(\tau) = \frac{\partial \Phi_1}{\partial \xi}\Big|_{\xi=o+} + r_1(\tau) - \frac{\partial \Phi_3}{\partial \zeta}\Big|_{\zeta=o-} \tag{28}$$

and

$$\frac{\partial \Phi_2}{\partial \xi}\Big|_{\xi=o+} = -\,2\,n(\tau)\left[\frac{Q(1-\chi)}{M_F\,\nu'_F\,L} + \frac{Y_{o\infty}\,Q(1-\chi)}{M_o\,\nu'_o\,L} - \Phi_2\Big|_{\xi=o+}\right] \tag{29}$$

The easiest way to solve these equations is to guess first that $\Phi_1(\xi,\tau)$, $\Phi_2(\xi,\tau)$, $\Phi_3(\zeta,\tau)$, $n(\tau)$ and $r_1(\tau)$ are all independent of τ, and then verify that the solution satisfies the original τ dependent problem.

The solution of Eq. 's (22), ignoring their time dependence is

$$\Phi_i(\xi) = \Phi_i(0)\,\frac{\operatorname{erfc}(\xi - n)}{\operatorname{erfc}(-n)} \quad ; \quad \text{for } i = 1,2 \tag{30}$$

where the boundary condition equation (24), has been used. In particular, using the boundary condition equation (27), one has

$$\Phi_1(\xi) = -B\,\frac{\operatorname{erfc}(\xi - n)}{\operatorname{erfc}(-n)} \tag{31}$$

Similarly, the solution to equation (23), with equations (25) and (26) is

$$\varphi_3(\zeta) = \frac{C_p\,(T_{vap} - T_\infty)}{L} \; \frac{\operatorname{erfc}\left[\sqrt{\frac{\lambda_\infty \rho_\infty C_{p_w}}{\lambda_w \rho_w C_p}}\, n - \sqrt{\frac{\lambda_w \rho_w C_{p_w}}{\lambda_\infty \rho_\infty C_p}}\, \zeta\right]}{\operatorname{erfc}\left[\frac{\lambda_\infty \rho_\infty C_{p_w}}{\lambda_w \rho_w C_p}\, n\right]} \tag{32}$$

Rate of Fuel Vaporization

Substituting equations (31) and (32) into equation (28), one arrives at the mass transfer relationship

$$2n = \frac{2B}{\sqrt{\pi}} \; \frac{\exp(-n^2)}{\operatorname{erfc}(-n)} + r_1$$

$$- \frac{C_p\,(T_{vap} - T_\infty)}{L} \sqrt{\frac{\lambda_w \rho_w C_{p_w}}{\lambda_\infty \rho_\infty C_p}} \; \frac{2}{\sqrt{\pi}} \; \frac{\exp\left[-\frac{\lambda_\infty \rho_\infty C_{p_w}}{\lambda_w \rho_w C_p}\, n^2\right]}{\operatorname{erfc}\left[\sqrt{\frac{\lambda_\infty \rho_\infty C_{p_w}}{\lambda_w \rho_w C_p}}\, n\right]} \tag{33}$$

This important equation relates the mass transfer n to the mass transfer driving "force" B, the radiative heat transfer r_1 and the thermal drain of the fuel bed.

The last (i.e. the thermal drain) term can be simplified by noting that $\frac{\lambda_\infty \rho_\infty C_{p_w}}{\lambda_w \rho_w C_p}$ lies between 10^{-4} and 10^{-2} for almost all types of solid or liquid fuels. For n not too large relative to unity, equation (33) is

$$2n \cong \frac{2B}{\sqrt{\pi}} \; \frac{\exp(-n^2)}{\operatorname{erfc}(-n)} + r_1 - \frac{C_p\,(T_{vap} - T_\infty)}{L} \sqrt{\frac{\lambda_w \rho_w C_{p_w}}{\lambda_\infty \rho_\infty C_p}} \; \frac{2}{\sqrt{\pi}} \tag{34}$$

This simplification implies that the term $\rho_w C_{p_w} v_w \frac{\partial T}{\partial y}$ in equation (9), which term describes the slow motion of the fuel bed toward the vaporizing surface, is negligible.

The function $\Phi_2(\xi)$ can be calculated by substituting equation (30) into equation (29) and then using equation (33) to evaluate $\Phi_2(0)$.

$$\Phi_2(\xi) = \frac{B\left[\frac{Q(1-\chi)}{M_F \nu'_F L} + \frac{Y_{o\infty} Q(1-\chi)}{M_o \nu'_o L}\right] \frac{\operatorname{erfc}(\xi - n)}{\operatorname{erfc}(-n)}}{B + 1 - \frac{r_1}{2n} + \frac{C_p (T_{vap} - T_\infty)}{2n L}\sqrt{\frac{\lambda_w \rho_w C_{p_w}}{\lambda_\infty \rho_\infty C_p}} \frac{2}{\pi} \frac{\exp\left[-\frac{\lambda_\infty \rho_\infty C_{p_w}}{\lambda_w \rho_w C_p} n^2\right]}{\operatorname{erfc}\left[\sqrt{\frac{\lambda_\infty \rho_\infty C_{p_w}}{\lambda_w \rho_w C_p}}\, n\right]}} \tag{35}$$

Flame Temperature

At the flame ($y = y_f$ or $\xi = \xi_f$), the fuel vapor and oxygen concentrations are zero. Therefore, equations (3) and (30) provide

$$\Phi_1(\xi_f) = \frac{C_p (T_f - T_\infty)}{L} - \frac{Y_{o\infty} Q(1-\chi)}{M_o \nu'_o L} = -\frac{B \operatorname{erfc}(\xi_f - n)}{\operatorname{erfc}(-n)} \tag{36}$$

where T_f is the flame temperature.

In addition, equations (5) and (30) provide

$$\Phi_2(\xi_f) = \frac{Y_{o\infty} Q(1-\chi)}{M_o \nu'_o L} = \Phi_2(0) \frac{\operatorname{erfc}(\xi_f - n)}{\operatorname{erfc}(-n)} \tag{37}$$

Combining equations (36) and (37), one obtains

$$C_p (T_f - T_\infty) = \frac{Y_{o\infty} Q(1-\chi)}{M_o \nu'_o}\left[1 - \frac{B}{\Phi_2(0)}\right]$$

Using equation (35) for $\Phi_2(0)$, the flame temperature becomes

$$C_p (T_f - T_\infty) = \frac{\frac{Q(1-\chi)}{M_F \nu'_F} - L + \frac{R_1(t)}{(\rho v)_{y=o}} + C_p (T_{vap} - T_\infty)\left\{1 - \frac{1}{n\sqrt{\pi}}\sqrt{\frac{\lambda_w \rho_w C_{p_w}}{\lambda_\infty \rho_\infty C_p}} \frac{\exp\left[-\frac{\lambda_\infty \rho_\infty C_{p_w}}{\lambda_w \rho_w C_p} n^2\right]}{\operatorname{erfc}\left[\sqrt{\frac{\lambda_\infty \rho_\infty C_{p_w}}{\lambda_w \rho_w C_p}}\, n\right]}\right\}}{1 + \frac{M_o \nu'_o}{M_F \nu'_F Y_{o\infty}}} \tag{38}$$

where equation (20) has been used for r_1. The numerator of equation (38) is the net heat released into the gas-phase temperature field while unit mass of fuel is burned. The denominator indicates the total mass of gas into which this heat is deposited when unit mass of fuel is burned.

Flame Position

Inverting equation (17) one has

$$y_f = 2\sqrt{D_\infty t}\int_0^{\xi_f} \frac{\rho_\infty}{\rho}\, d\xi$$

Now using equations (8) and (3) this becomes

$$y_f = 2\sqrt{D_\infty t}\int_0^{\xi_f} \frac{T}{T_\infty}\, d\xi = 2\sqrt{D_\infty t}\,\frac{L}{T_\infty C_p}\int_0^{\xi_f}\left[\Phi_1(\xi) + \frac{Y_{O\infty} Q(1-\chi)}{M_O \nu_O' L} + 1\right] d\xi$$

which can be integrated to obtain

$$y_f = 2\sqrt{D_\infty t}\left\{\frac{T_{vap}}{T_\infty}\,\xi + \frac{BL}{C_p T_\infty}\left[(\xi_f - n)\left(1 - \frac{\operatorname{erfc}(\xi_f - n)}{\operatorname{erfc}(-n)}\right) - \frac{1}{\sqrt{\pi}}\,\frac{\left[e^{-n^2} - e^{-(\xi_f - n)^2}\right]}{\operatorname{erfc}(-n)}\right]\right\} \qquad (39)$$

One sees, from this equation, that the distance between the flame and fuel bed increases directly with $\sqrt{t}$. To evaluate y_f numerically, one can determine ξ_f from equation (37) using the value of $\Phi_2(0)$ from equation (35).

Burning Rate at the Flame

Define $-\dot{m}''_F$ as the rate per unit area with which fuel is consumed at the flame sheet. From equation (2) one obtains

$$\dot{m}''_F = \int_{y_{f-}}^{y_{f+}} \dot{m}'''_F \, dy = \int_{y_{f-}}^{y_{f+}} \left\{ \rho \frac{\partial Y_F}{\partial t} + \rho v \frac{\partial Y_F}{\partial y} - \frac{\partial}{\partial y} \left(\rho D \frac{\partial Y_F}{\partial y} \right) \right\} dy$$

Using equation (17) to transform y to ξ and then integrating, one obtains, (noting that $Y_F(\xi)$ is continuous)

$$\dot{m}''_F = \frac{\rho_\infty}{2} \sqrt{\frac{D_\infty}{t}} \left. \frac{\partial Y_F}{\partial \xi} \right|_{\xi_{f-}}$$

or, in terms of Φ_2

$$\begin{aligned} \dot{m}''_F &= \frac{\rho_\infty}{2} \sqrt{\frac{D_\infty}{t}} \frac{M_F \nu'_F L}{Q(1-\chi)} \left. \frac{\partial \Phi_2}{\partial \xi} \right|_{\xi_{f-}} \\ &= - \rho_\infty \Phi_2(0) \sqrt{\frac{D_\infty}{\pi t}} \frac{M_F \nu'_F L}{Q(1-\chi)} \frac{e^{-(\xi_f - n)^2}}{\operatorname{erfc}(-n)} \end{aligned} \tag{40}$$

Flame Radiation

It was assumed in the formulation that the radiation is proportional to the rate of combustion. That is the rate of radiant energy release per unit volume $\dot{q}'''_{rad} = \chi \dot{q}'''_{chem} = \frac{-\chi Q \dot{m}'''_F}{M_F \nu'_F}$. Therefore, the rate of radiant energy release per unit flame area, $\dot{q}''_{rad}$ equals

$$\dot{q}''_{rad} = \int_{y_{f-}}^{y_{f+}} \dot{q}'''_{rad} \, dy = \frac{-\chi Q \dot{m}''_F}{M_F \nu'_F}$$

or, using equation (40)

$$\dot{q}''_{rad} = \frac{\chi L}{1-\chi} \rho_\infty \Phi_2(0) \sqrt{\frac{D_\infty}{\pi t}} \frac{e^{-(\xi_f - n)^2}}{\operatorname{erfc}(-n)} \tag{41}$$

If the gases are transparent, and if half of the radiation is directed toward the fuel bed, then the radiative heat transfer received by the fuel bed per unit area, $R_1(t)$, will be

$$R_1(t) = \frac{1}{2} \epsilon \dot{q}'''_{rad} = \frac{\chi \epsilon L \rho_\infty \Phi_2(0)}{2(1-\chi)} \sqrt{\frac{D_\infty}{\pi t}} \frac{e^{-(\xi_f - n)^2}}{\operatorname{erfc}(-n)} \tag{42}$$

where ϵ is the emissivity of the fuel bed. Thus

$$r_1 \equiv \frac{2R_1(t)}{L\rho_\infty} \sqrt{\frac{t}{D_\infty}} = \frac{\chi \epsilon}{1-\chi} \frac{1}{\sqrt{\pi}} \Phi_2(0) \frac{e^{-(\xi_f - n)^2}}{\operatorname{erfc}(-n)} \tag{43}$$

Equation (43) shows that r_1 is independent of time. This verifies our assumption made in the paragraph following equation (21), since from equation (33) we already know that n is independent of time if r_1 is also independent of time.

2.2.4 Summary and Conclusions

The transient problem was formulated and then transformed to a similarity problem. This transformation also converted the temperature dependent properties (density, diffusivity and conductivity) to their ambient values. By assuming that the flame radiation is proportional to the rate of combustion, it was possible to solve for: the rate of mass transfer, $(\rho v)_{y=o} = n \rho_\infty \sqrt{\frac{D_\infty}{t}}$, equation (33); the flame temperature, T_f, equation (38); the flame position, y_f, equation (39); the rate of fuel consumption at the flame, $\dot{m}''_F$, equation (40); and finally the radiative heat transfer, $R_1(t)$, equation (42).

The previous equations show that: y_f increases with the square root of time; T_f is constant; and $(\rho v)_{y=o}$, $\dot{m}''_F$, and R_1 (t) decrease inversely with the square root of time. These results are what one might intuitively expect with the approximation of $\dot{q}'''_{rad} = \chi \dot{q}'''_{chem}$ made in Section 2.2.2.

A consideration of equation (33) shows that if $n > 0$, a flame will propagate away from the fuel bed. However, if $n \leq 0$, no flame will occur because too much heat is absorbed by the fuel bed interior. It can also be seen from eq. (33) that the critical condition, n = 0, occurs when

$$0 = \frac{2\,B}{\sqrt{\pi}} + r_1 - \frac{C_p\,(T_{vap} - T_\infty)}{L} \sqrt{\frac{\lambda_w\,\rho_w\,C_{pw}}{\lambda_\infty\,\rho_\infty\,C_p}} \quad \frac{2}{\sqrt{\pi}}$$

When n = 0 there will be no mass transfer, and thus no radiation i.e. $r_1 = 0$. The critical condition becomes

$$B \equiv \frac{Y_{O\infty}\,Q\,(1-\chi)}{M_O\,\nu'_O\,L} - \frac{C_p\,(T_{vap}-T_\infty)}{L} = \frac{C_p\,(T_{vap}-T_\infty)}{L} \sqrt{\frac{\lambda_w\,\rho_w\,C_{pw}}{\lambda_\infty\,\rho_\infty\,C_p}}$$

For most fuels burning in air, the term $\frac{C_p\,(T_{vap}-T_\infty)}{L}$ is generally much smaller than the mass transfer driving "force" B. Thus, the critical condition is approximately

$$\frac{Y_{O\infty}\,Q\,(1-\chi)}{M_O\,\nu'_O\,C_p\,(T_{vap}-T_\infty)} \sqrt{\frac{\lambda_\infty\,\rho_\infty\,C_p}{\lambda_w\,\rho_w\,C_{pw}}} \cong 1 \qquad (44)$$

This last equation should provide an estimate of the flammability of fuels in a zero gravity field.

Equation (34) was used to calculate the mass transfer number, n, for several typical liquid fuels burning at zero g in pure oxygen at

1/3 atm and in air at 1 atm. The radiation term, r_1, was neglected as a first approximation. Later, it was included for one particular fuel.

The calculations showed that, when radiation is neglected, alcohols ranging between CH_3OH and C_4H_9OH, and paraffins ranging between CH_4 and C_8H_{18} should burn (i.e. $n > 0$) in the pure oxygen atmosphere. On the other hand, no alcohols will burn (i.e. $n < 0$) in air at 1 atmosphere while paraffins falling between CH_4 and C_5H_{12} will burn.

A typical value for n = 0.59 was calculated for C_2H_5OH in pure O_2 at 1/3 atm. By employing the definition of n as given in equation (21), the fuel vaporization rate at the surface, $(\rho v)_{y=o}$, becomes

$$(\rho v)_{y=o} = 0.59\, \rho_\infty \sqrt{\frac{D_\infty}{t}}$$

$$\approx \frac{.0001}{\sqrt{t}} \qquad g/cm^2 s$$

(It should be pointed out that time t begins after ignition had already occurred by some mechanism such as a high energy pulse.)

The effect of including the radiation term on the burning rate was studied for C_8H_{18} in pure O_2 and 1/3 atm. It was assumed that 20% of the chemical energy liberated is radiated and that 50% of this energy went back to the fuel bed. The result was a slight decrease in n from 0.26 to 0.24. This implied that heat transfer by conduction back to the fuel was a slightly more efficient mechanism than radiation. However, when 100% of the radiation was assumed to go back to the fuel, the value of n increased to .475. This would be expected since the total heat transfer back to the fuel had been definitely increased.

There are no experimental data with which to compare the predicted burning rates. As pointed out earlier, this theory is strictly

applicable to a flat fuel where the dominant extinguishing mechanism is the thermal drain from the flame into the cold fuel bed interior. Kumagai and Isoda's [2,3] experiments, for instance, were limited to small spherical droplets which reach thermal equilibrium very early in the combustion process and thus offer minimal thermal drain from the flame. Thus, it is not surprising to note that both heptane and ethyl alcohol droplets did burn in air at 1 atm while this theory predicts that they do not.

2.3.1 Previous Work

Qualitative observations of small fires under actual zero gravity conditions were reported by Kimzey et al[5], Hall[4] and Stevens et al[6].

Kimzey photographed the combustion of different pieces of polymers and paraffin during short periods of weightlessness in airplane flights of parabolic trajectory. His cine film of the combustion of paraffin showed that after a visible extinction of the flame at 0.84 seconds after ignition and a period of 4.25 seconds of darkness, the flame reappeared. This was due to either a return to gravity or the collision of the combustion chamber with the aircraft wall.

Stevens et al[6] burned small samples (3.2 x 0.6 x 0.3cm) of polyethylene in pure and diluted oxygen atmospheres (at 256-569 mm Hg) in the same combustion chamber used by Kimzey. The times for burnout under zero gravity conditions were found to be roughly 50% higher than in normal gravity. This result agrees qualitatively with results obtained by Kumagai and Isoda[2,3] who measured burning rates in air of suspended fuel droplets (n-heptane and ethyl alcohol), flame diameters and hot gas diameters in gravitational fields varying between zero and one-g, produced in a falling chamber. They found that, regardless of the gravitational field strength, the known relationship between the mass burning rate and the droplet diameter for diffusion flames is valid.

$$\dot{m} = \alpha d \tag{45}$$

Where $\dot{m}$ = mass burning rate (g/s)

d = fuel drop diameter (cm)

α = proportionality constant.

This means that the related expression for the decrease of droplet size with time also holds.

$$d_o^2 - d^2 = kt \tag{46}$$

Where t = time (s)

d_o = initial fuel drop diameter (cm)

k = fuel evaporation constant (cm^2/s).

However, k was found to increase considerably when gravity varied from zero to one-g. Values for n-heptane and ethyl alcohol were respectively 0.0049 and 0.0046 cm^2/s at zero-g and 0.010 and 0.0075 cm^2/s at one-g.

Kumagai and Isoda made an attempt to measure the visible flame diameter and the diameter of the hot gas sphere. Whereas the flame diameter reached a maximum after about 0.5 seconds (the free fall height was only 5m), the hot gas diameter as observed by schlieren photography increased initially as the square root of time and later at slower rates. For droplet sizes of 0.1cm, the flame diameter had increased to 2cm after 0.1 second.

Cocran[8] is preparing experiments at NASA-Lewis for studying the behavior of low momentum fuel jet diffusion flames and the flammability characteristics of various materials under zero-g conditions. Two drop towers are available for zero-g simulation. One is 26m high and is used for preliminary experiments and the other is 152m high equipped with pumping facilities so that free fall can be studied in vacuum. The maximum period of weightlessness available with the 152m drop tower is eleven seconds. No studies are under way or planned at this time for determining flame extinguishment time or maximum flame thickness.

Obviously, steady state combustion of a flat surface is not possible in the absence of natural convection. The increasing thickness of the layer of combustion products which separates the fuel from the surrounding oxidant increases the time for the diffusion mixing process of a stoichiometric unit of fuel and oxidant. When the rate of energy loss due to radiation and to conduction outweighs the rate of energy

release by combustion, the flame will be extinguished. The determination of the factors governing the characteristic self-extinguishment time and the thickness of the final layer of hot gases having a temperature just below the ignition temperature is of special interest to the space-craft fire hazard.

Kumagai and Isoda had neither enough fuel nor time for measuring the final flame thickness and extinguishment time. On the other hand, small perturbations during weightlessness may have prolonged the lifetime of the flame during Kimzey's experiments without being visible to the cine camera.

The remainder of this section is devoted to a description of theoretical and experimental models which were employed to simulate the essential phenomena occurring during zero-g combustion.

2.3.2 Radiative Cooling of Diffusion Flames

2.3.2.1 Introduction

The mathematical model described in section 2.2 predicted that during zero-g combustion of a flat surface, the temperature of a non-radiative flame should remain constant with time. This was also true for a flame in which the rate of radiative energy release was proportional to the rate of combustion energy generation. These concepts are physically unrealistic. The rate of radiation should increase with time in the initial stages of the combustion process due to an increase in the product gas layer thickness while the flame temperature should decrease.

Because of the importance of the radiative cooling process of combustion products during zero-g burning, the extinguishment times of diffusion flames due to radiation alone were calculated. These provide an upper limit for extinguishment time since the presence of conduction helps speed the extinguishment process. Two cases were considered:

(i) Cooling of a semi-infinite hot gas layer of constant thickness

(ii) Cooling of a flat-diffusion flame of increasing thickness.

The reason that the second case was considered was that a flat steady state diffusion flame can be used to simulate zero-g combustion quite effectively. The transient combustion process present in zero-g is replaced by a progressive change in thickness in the vertical direction brought about by the same physical diffusion mechanism present in zero-g transient flames. This is discussed further in paragraph 2.3.2.3.

In both cases, the radiating gases were assumed to be composed entirely of CO_2, H_2O and a reasonable quantity of soot equal to 10^{-6} volume fraction. The emissivity of the gaseous mixture, ϵ_g, was found by using the methods described by Hottel and Sarofim[9]. The soot emissivity, ϵ_s, wascalculated from the relation[9]

$$\epsilon_s = 1 - \left[\frac{1}{1 + K f_v LT}\right]^4 \qquad (47)$$

Where $K \cong 5.2\ cm^{-1}\ {}^oK^{-1}$ recommended for a pure carbon soot

f_v = volumetric fraction occupied by the soot particles

L = flame thickness (cm)

T = flame temperature (^oK)

Assuming gray gas behavior, that Kirchoff's Law applies and that soot particles are non-reflective, the total emissivity of the flame, ϵ_f, was calculated by the equation[10]

$$\tau_f = 1 - \epsilon_f = \tau_g \tau_s = (1 - \epsilon_g)\ (1 - \epsilon_s)$$

$$\text{or}\quad \epsilon_f = \epsilon_g + \epsilon_s - \epsilon_g \epsilon_s \qquad (48)$$

Where τ_f = transmissivity of the flame

τ_g = transmissivity of the gas

τ_s = transmissivity of the soot

2.3.2.2 Cooling of a Gas Layer of Constant Thickness

The energy balance for a hot gas layer which is radiating heat to the surroundings is

$$- AL\, C_p \rho \frac{dT}{dt} = 2\epsilon_f \sigma (T^4 - T_o^4)\, A$$

Where A = area of one face of the flame (cm^2)

T_o = temperature of the surroundings (^oK)

The time required by the layer to cool from T_1 to T_2 can be found by integration.

$$t = \int_{T_2}^{T_1} \frac{L\, C_p\, \rho}{2\epsilon_f \sigma (T^4 - T_o^4)}\, dT \qquad (49)$$

The time required by the hot combustion products of a stoichiometric mixture of CH_4 and oxygen at 1 atm to cool down from an initial temperature of 3000^oK to an arbitrary low value of 500^oK (i.e. below the ignition temperature) was calculated for different thicknesses. The solution of equation (49) required graphical integration because of the dependence of C_p, ρ, ϵ_f on temperature and of ϵ_f on flame thickness L. A typical graphical integration is shown in Figure 2. These calculations were repeated for a C_3H_8 - O_2 mixture and for a platinum sheet. Upon inspection of the results which are presented in Figure 3, the following observations can be made:

(i) For the same thickness, the change in composition between one hydrocarbon and another does not affect the rate of temperature decrease appreciably.

(ii) As expected, longer cooling times are necessary for gas layers of greater optical thickness. For optically thin layers, one would expect cooling times to be only dependent on the probability of spontaneous emission for the different molecular states involved and not

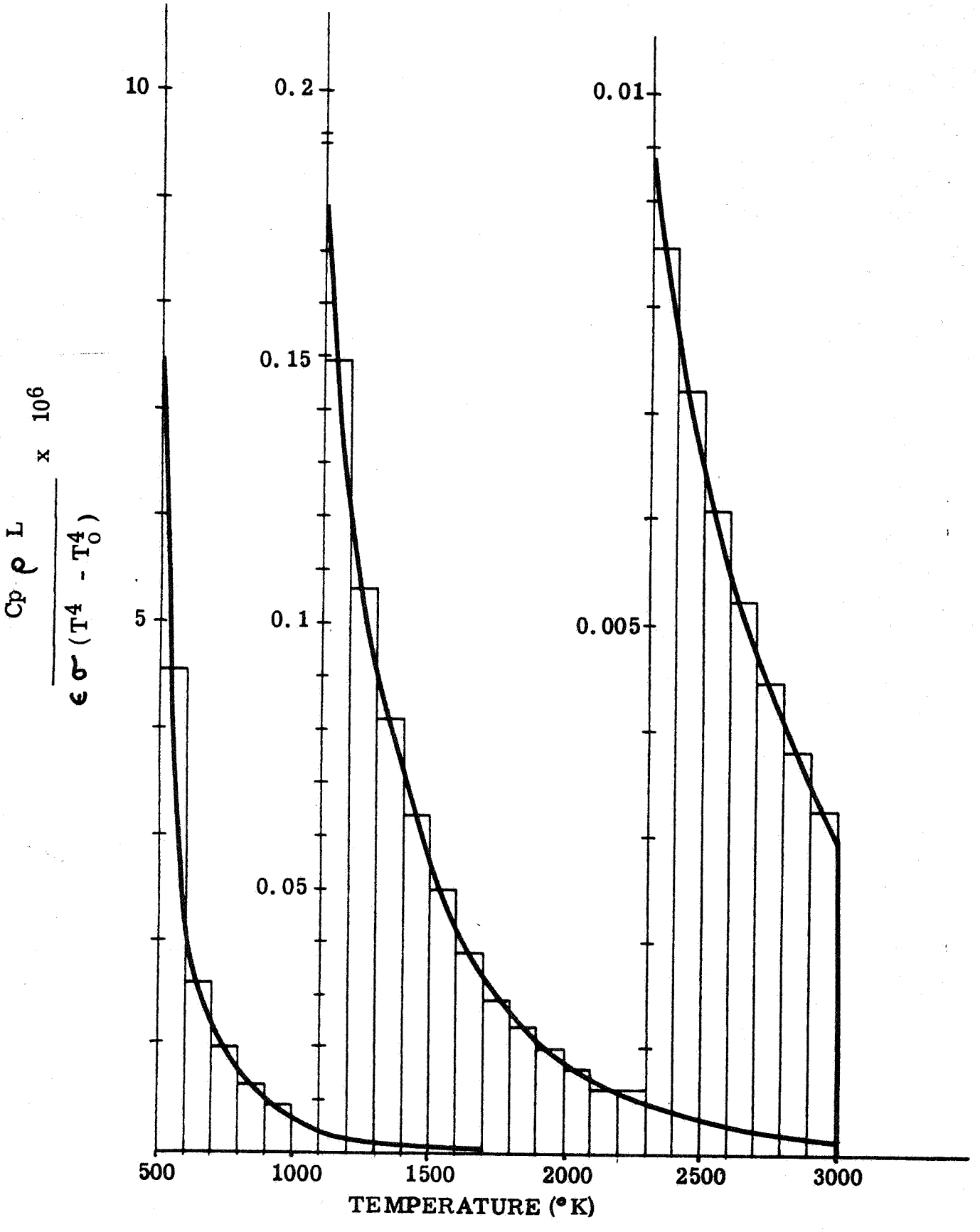

Fig. 2 Determination of the time, t, required for cooling of a 1 cm thick layer of CH_4-O_2 Flame product gases.

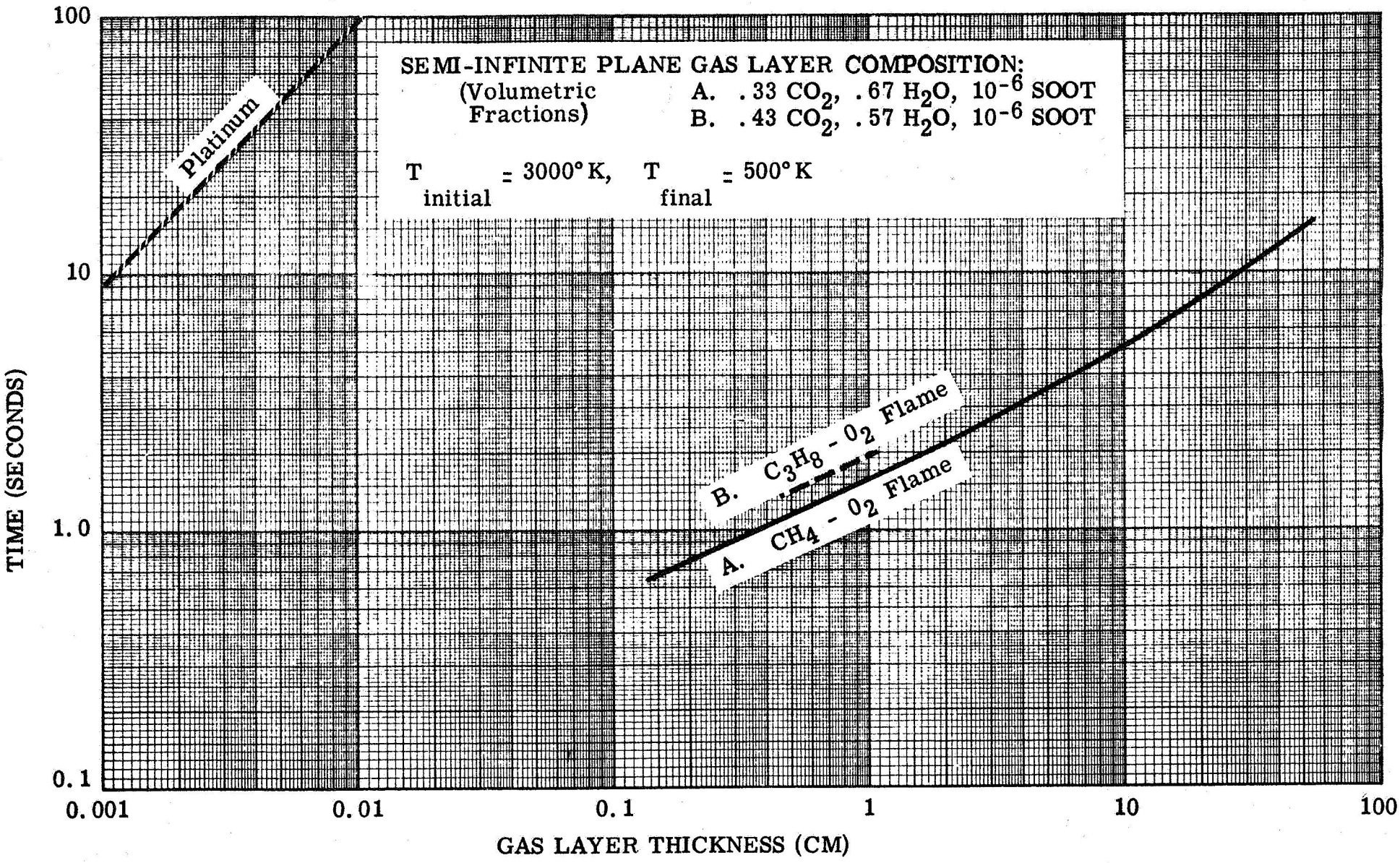

Fig. 3 - Time required for CH_4-0_2 and C_3H_8-0_2 flame product gases in layers of varying thickness to cool by radiation only below ignition temperature. The cooling curve for a platinum layer is included for comparison.

on the layer thickness. The much longer cooling times required by platinum are consistent with its much higher volumetric specific heat.

(iii) The cooling time is mainly determined by the radiative properties of the layer at low temperatures. Thus, the total energy radiated to the surroundings while cooling from $3000^{o}K$ to $500^{o}K$ is roughly equal to the energy radiated at $800^{o}K$ during the same period of time.

(iv) The magnitude of the calculated times indicate that the results are amenable to experimental verification.

2.3.2.3 Cooling of a One Dimensional Transient Diffusion Flame

As stated earlier, the flat laminar diffusion flame can be used effectively to simulate zero-g combustion. A burner of this type employs unburned fuel and oxidizer flowing in a verical upward direction with the flame at the interface[11]. The flow field distortion introduced by buoyancy does not alter the diffusive mixing of fuel and oxidant appreciably. Combustion products accumulate between the fuel and oxidant sources thus simulating zero-g combustion. However, unlike the model described in the previous paragraph, a flat diffusion flame will have an increasing thickness due to diffusion and accumulation of combustion products and a flame temperature which decreases with height. Before describing the experiments with flat diffusion flames, it is necessary to consider a more realistic model for radiative cooling from such a flame.

A theoretical model resembling a flat (laboratory) diffusion flame was considered. It should be reiterated that this model also describes the transient zero-g diffusion flame. The following assumptions were made:

(i) A semi-infinite amount of oxidant flowing upwards parallel to and unmixed with a semi-infinite stream of gaseous fuel.

(ii) After ignition, a flat diffusion flame is obtained, the thickness of which increases with height according to the relation

$$L = \sqrt{2 D_\infty t}$$

where $t = \frac{z}{v}$ (s)

z = height (cm)

v = average velocity within the flame (cm/s)

D_∞ = mass diffusivity in the surroundings (cm^2/s)

(iii) A Lewis number equal to one. Since this number is the ratio of thermal to mass diffusivity, the thickness L will describe the temperature as well as the combustion products layer thickness.

(iv) As soon as the fuel and oxidant enter the layer, the heat of combustion is released and used to heat the layer uniformly.

An overall heat balance can be written for a differential element of the flame at a height z, where the flame thickness is L and the temperature is T.

$$\rho C_p L (T - T_o)\, dA = H (\rho L\, dA) - dA \int_o^t 2 \epsilon \sigma (T^4 - T_o^4)\, dt$$

or

$$T = \left(T_o + \frac{H}{C_p}\right) - \frac{2}{\rho C_p L} \int_o^t \epsilon \sigma (T^4 - T_o^4)\, dt \qquad (50)$$

Substituting for $T_o + \frac{H}{C_p}$ the adiabatic flame temperature T_f and rewriting equation (50) in a form suitable for numerical solution, one arrives at

$$T_n = T_f - \frac{2}{\bar{\rho}_n \bar{C}_{pn} \bar{L}_n} \sum_{i=o}^{n} \bar{\epsilon}_i \sigma (\bar{T}_i^4 - T_o^4) \Delta t_i \qquad (51)$$

where $\bar{T}$, $\bar{\epsilon}$, $\bar{\rho}$, $\bar{C}_p$, $\bar{L}$ are average values for the gases in element Δz corresponding to time interval Δt.

Since $\bar{L}_n = \sqrt{2\bar{D}_n t_n}$

and $D_n \sim T_n^{1.8}$

$\rho_n \sim T_n^{-1}$

$C_{p_n} \sim$ roughly a constant

The product $\bar{C}_{p_n}\bar{\rho}_n\sqrt{2\bar{D}_n}$ is proportional to $T_n^{-0.1}$. This term was thus considered a constant in the numerical iterative procedure used to solve equation (51).

Starting with the adiabatic flame temperature T_f, a temperature T_1 is calculated after time t_1 has elapsed by trial and error. This is done by estimating a $\bar{T}_1$ between T_1 and T_f and an average gas layer thickness $\bar{L}_1 \simeq \sqrt{2\bar{D}_1 t_1}$ for calculating ϵ_1. Consecutive temperatures T_n are obtained in a similar manner. The procedure is simplified by plotting T_n vs t_n continuously in order to arrive at better first estimates of T_{n+1} by successive extrapolation. The resulting curves were found to be relatively independent of the iteration step sizes (t_{n+1}/t_n) which were varied between 10 and $10^{1/4}$. Plots showing the decrease in temperature with time (corresponding to height) for CH_4-O_2 and CH_4-Air flat flames are presented in Figures 4 and 5. Figure 6 shows the variation of the flame thickness with time (height) while Figure 7 represents the variation of the rate of thermal radiation with time.

A comparison of Figures 4 and 5 indicates that there is little difference between the times (0.65 s in O_2 vs. 0.25 s in air) taken to reach 1000°K when one might expect visible flame extinguishment. The curves were continued to about 500°K at which most normal solid fuels are difficult to ignite. Figure 6 shows that the final flame product layer thickness at that temperature is of the order of 10 cm. Figure 7 shows the expected course of radiative losses from the flame which

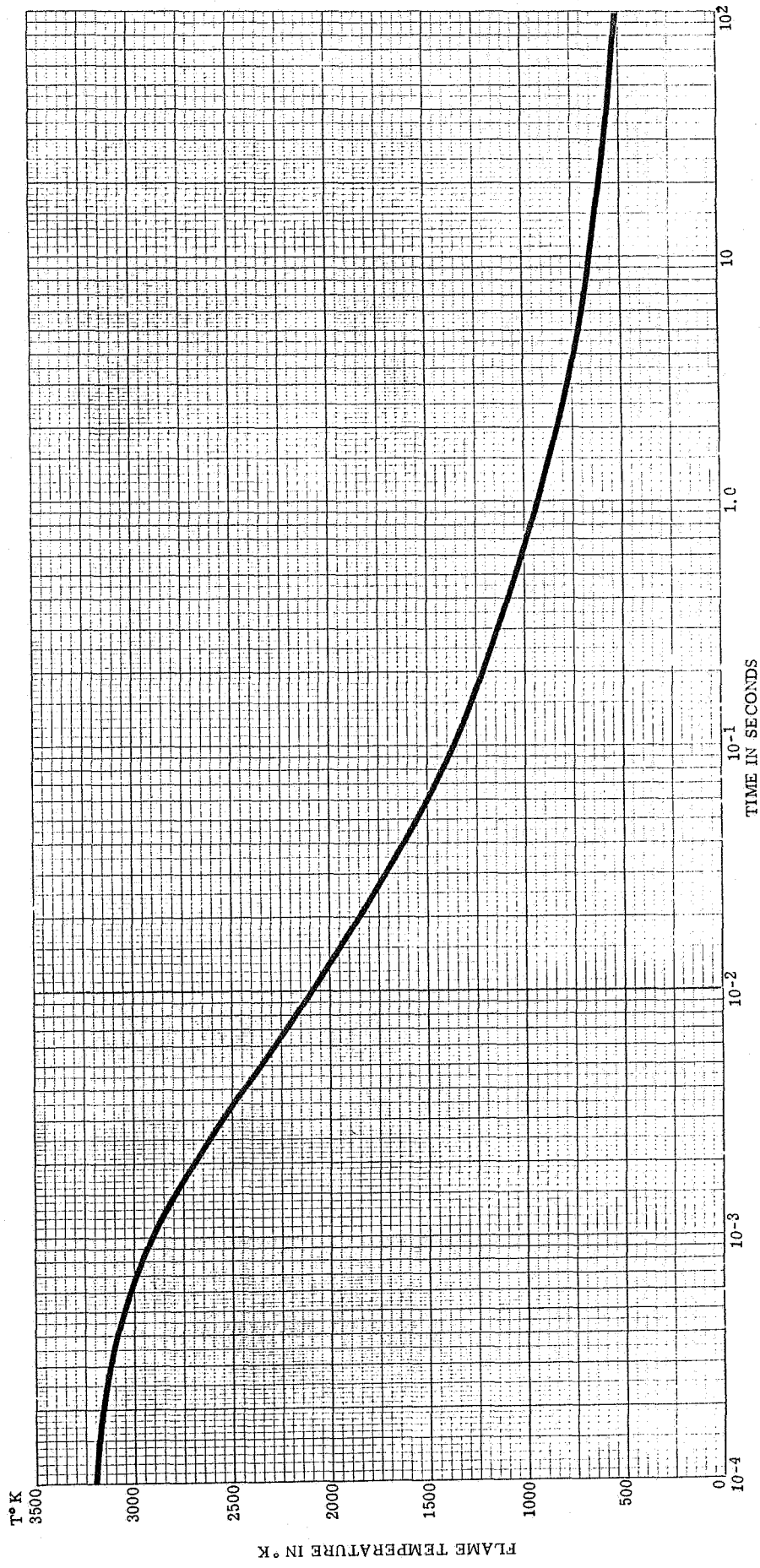

Fig. 4 - Cooling of a CH_4 - O_2 one dimensional diffusion flame by radiative heat loss

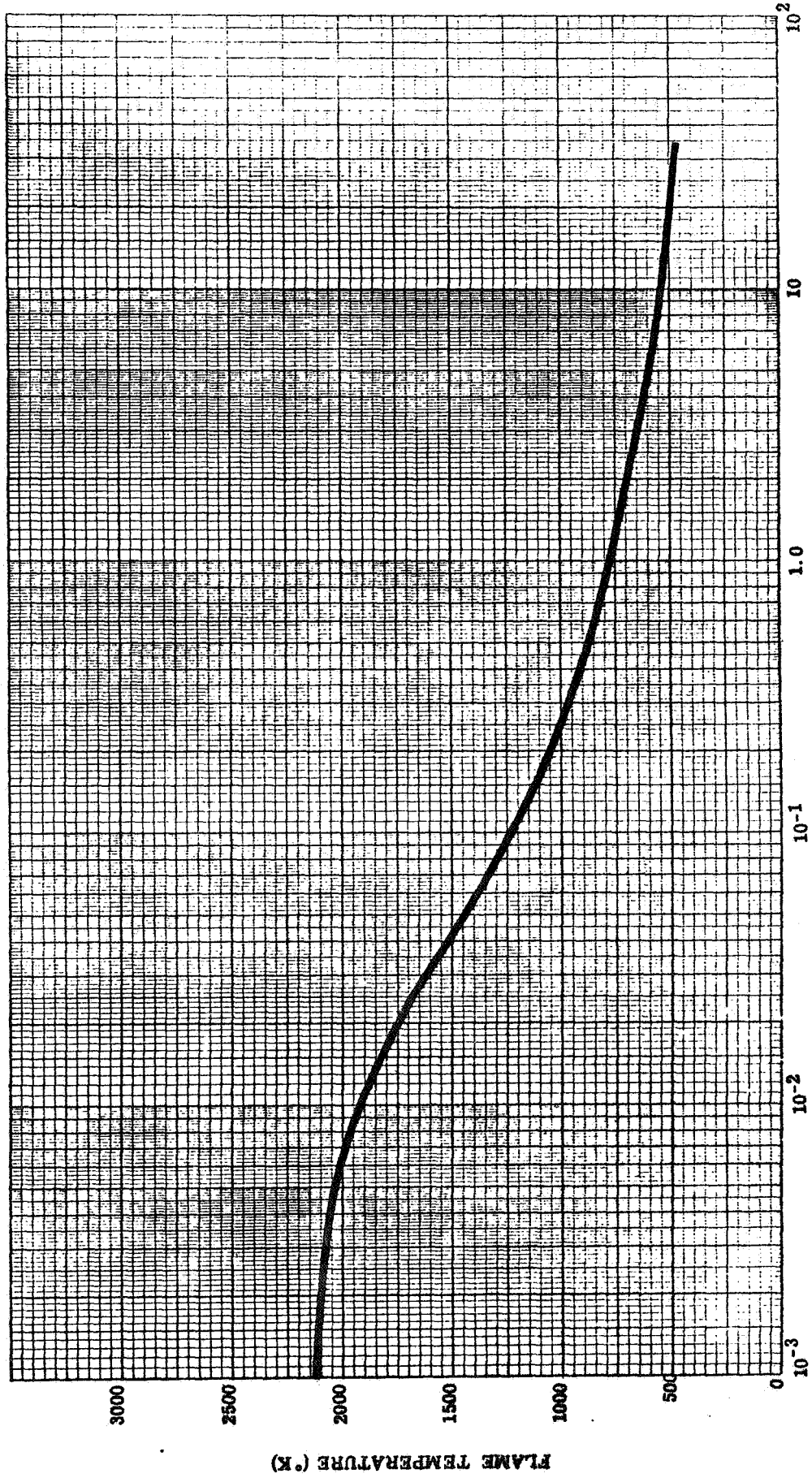

Fig. 5 - CH_4-Air Diffusion Flame Cooling by Radiative Heat Loss

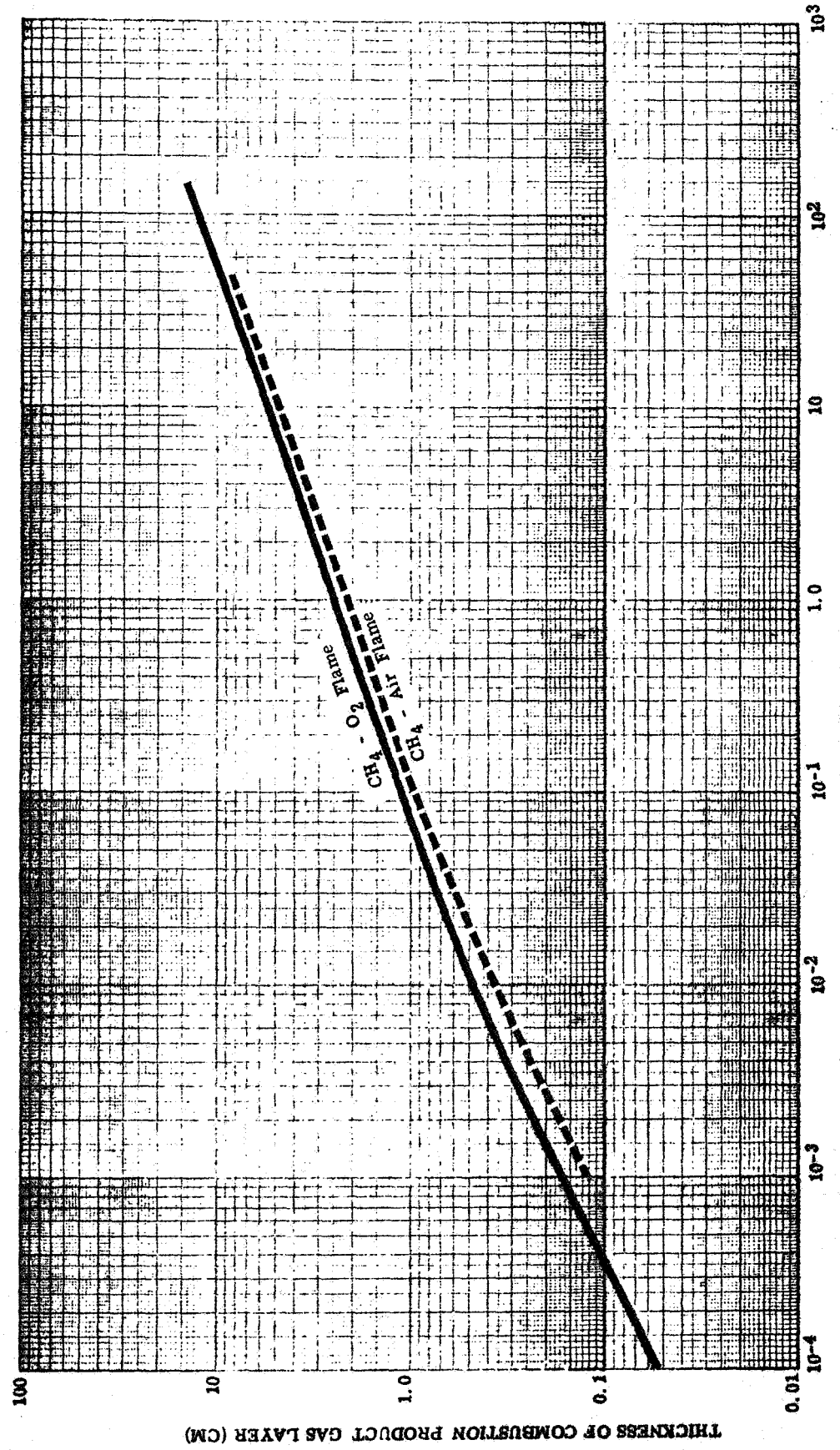

Fig 6 - Increase of the flame gas layer thickness with time

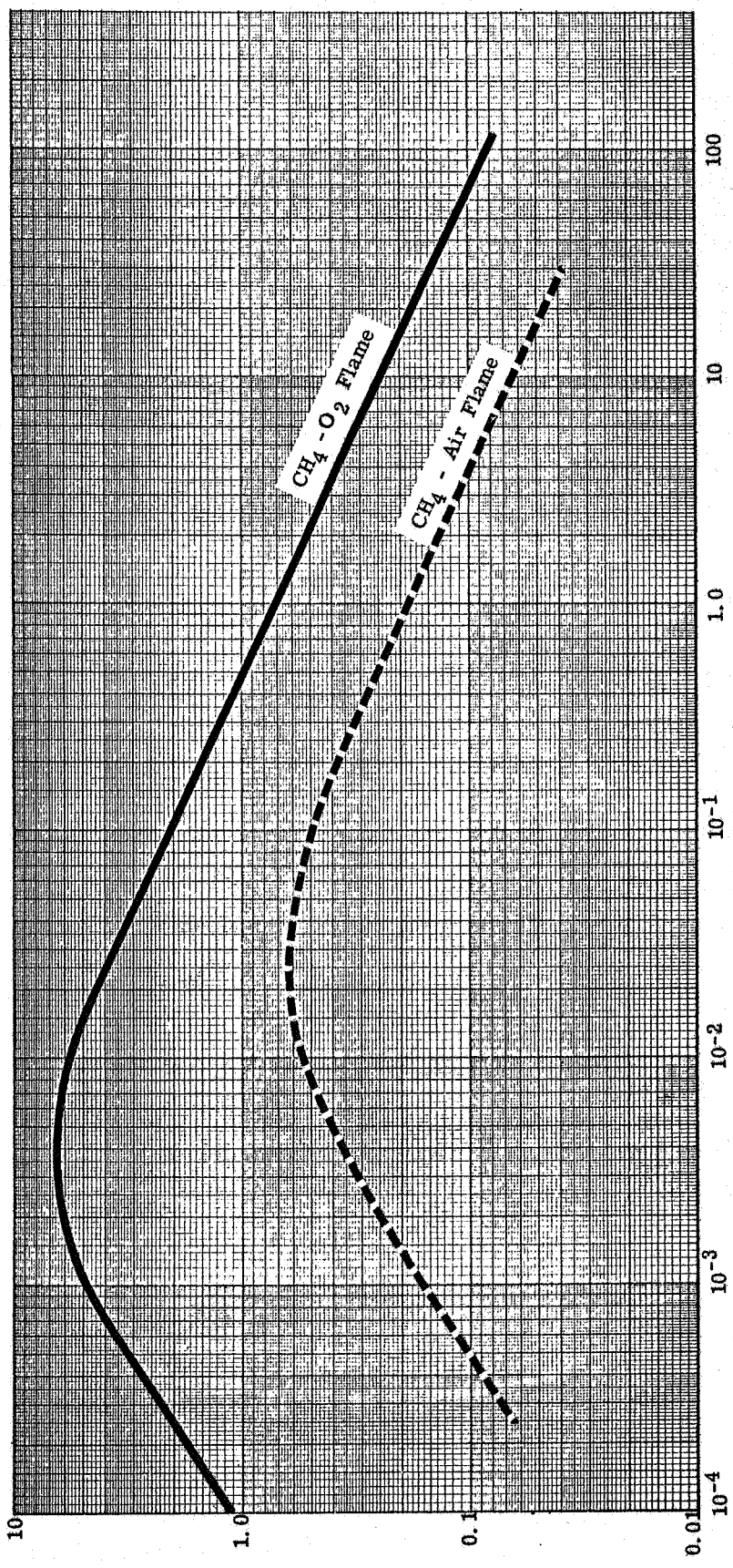

Fig. 7 - Radiative heat loss rate of CH_4 flames as a function of time after ignition

begins at low rates because of the small initial radiating thickness, increases to a maximum and then decreases as the influence of decreasing temperature predominates over the increasing gas layer thickness.

2.3.3 Experimental Study of Radiant Extinction of Flat Diffusion Flames

2.3.3.1 Introduction

The flat diffusion flame which can be sustained between parallel upward flows of fuel and oxidant presents an effective means for simulating the essential phenomena occurring during zero-g combustion. Although the presence of gravity distorts the initial uniform flow field because of the hot central flame, these buoyancy effects are measurable and do not alter the basic fuel-oxidant diffusive mixing process.

2.3.3.2 Description of Apparatus

A flat diffusion flame burner was constructed from sheet metal with a Pyrex glass front to permit observation. A diagram of the burner with an approximate scale and a photograph of the apparatus are shown in Figures 8 and 9. Porous metal plates were used to eliminate turbulence of the ensuing fuel and oxidant streams. Nitrogen was employed as a shield gas. The dimensions of the apparatus were chosen so that the nitrogen characteristic diffusion length was about 7 cm. Since the diffusion length $X \simeq \sqrt{2Dt}$ and $D_{CH_4\text{-}N_2}$ at 1800°K is about 2.25 cm^2/s, the allowable observation time was of the order of 10 seconds. This period was much longer than the expected flame extinguishment time.

Care had to be taken in order to insure the stabilization of the flame. The following procedures were found to improve stabilization:

1. An approximately stoichiometric flow of fuel and oxidizer were used to obtain a vertical flame.
2. Nearly identical flow velocities were used on both sides.
3. Better stabilization was obtained when both the fuel and oxidizer gases had about the same radiation absorbing characteristics. This was achieved by injecting a small amount of CO_2 into the oxidizer stream.

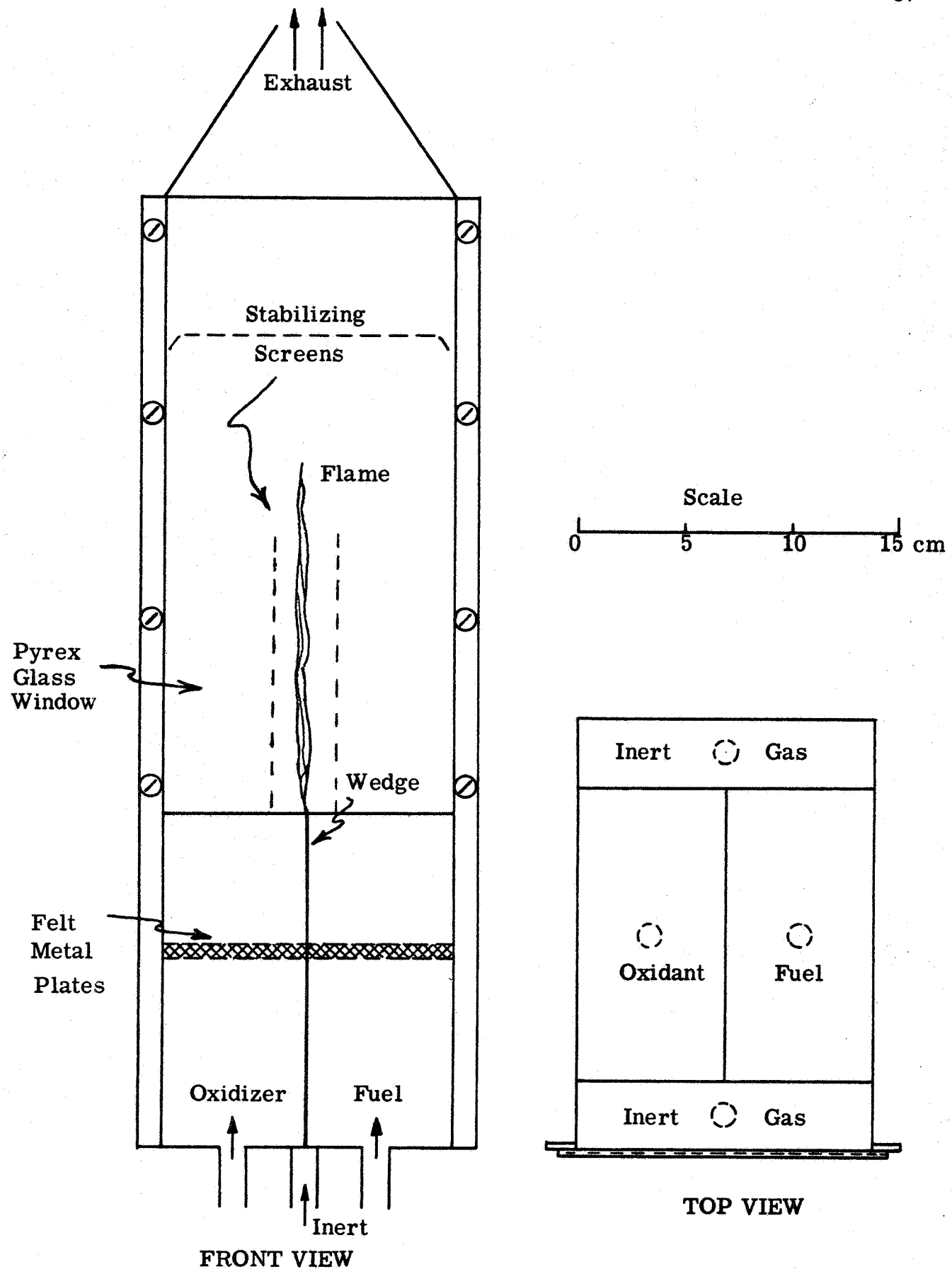

FIG. 8 "FLAT" DIFFUSION FLAME BURNER

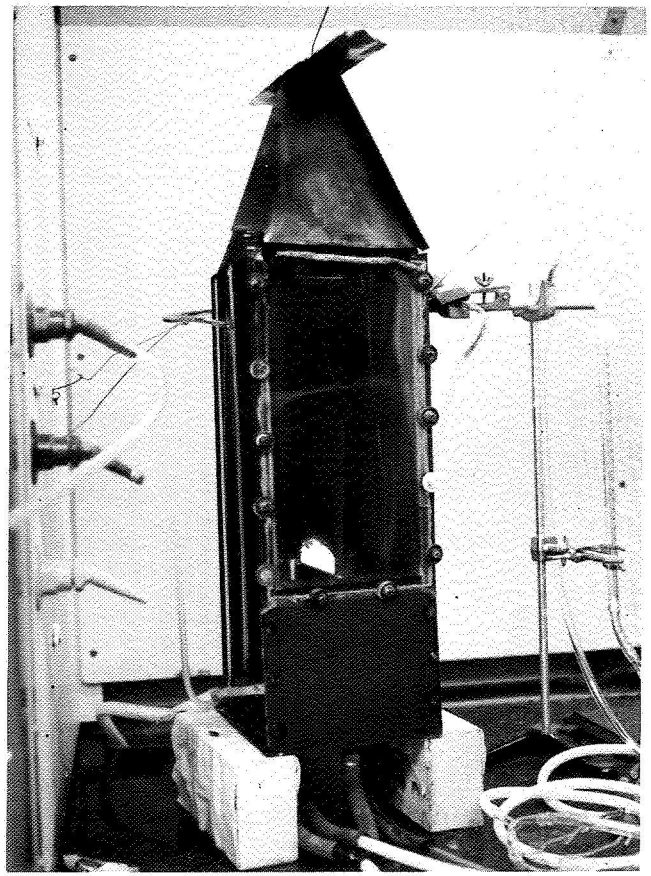

Figure 9 Photograph of the flat diffusion flame burner

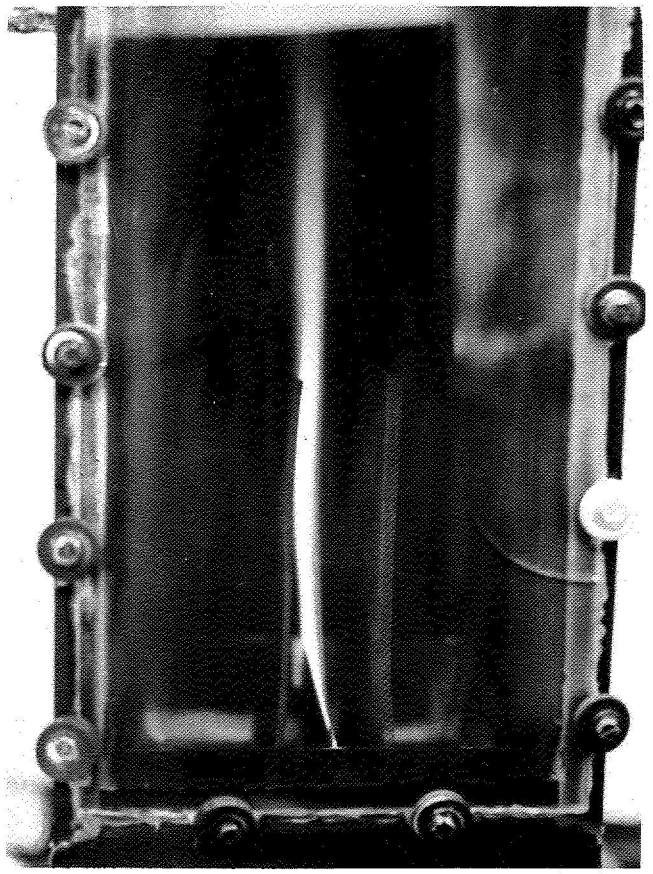

Figure 10 Close-up of a flat flame stabilized between two screens, 3 cm apart $v_o \approx 4.5$ cm/s

4. Flow velocities greater than 2.5 cm/s had to be used in order to avoid excessive deformation of the flow field due to entrainment of cold gases into the central flame zone. At lower velocities, an undesirable circulation flow pattern was established.
5. The upper limit on velocity was set by the available gas supply, the finite height of the chamber and the desire to have a laminar flame.
6. A horizontal metal screen placed near the exhaust (see Fig. 8) was found to reduce undesirable recirculation patterns. The presence of two screens parallel to the flame was found to improve the stability of the flame considerably. The contribution of these screens in stabilizing the laminar flame outweighs their detrimental effect on the thermal radiation and mass diffusion rates.

2.3.3.3 Experimental Results

A flame similar to that shown in Fig. 10 was used to estimate the radiative extinguishment time. The fuel stream consisted of 87 cm^3/s CH_4, 38 cm^3/s C_3H_8 and 320 cm^3/s N_2. The oxidant stream composition was 440 cm^3/s air and 25 cm^3/s CO_2. The shield gas consisted of 200 cm^3/s N_2 on each side. With an inlet area of 98 cm^2 on each side, the average linear velocity of fuel and oxidant streams was $\simeq$ 4.6 cm/s.

Since buoyancy causes entrainment in both the perpendicular as well as the flame plane itself, the flame tends to become higher in the center. Thus, an average flame height had to be estimated. Assuming that the cold gas linear velocity, v_o, was increased by a factor $T_{flame}/T_{room} \simeq 6$ due to expansion in the flame, and using the measured

average flame height of 12 cm, an extinguishment time of about 0.5 second was obtained. Probably, a more rigorous method for estimating flame velocity (such as the particle track method) should have been used, but the final result could not have been altered very much.

2.3.3.4 Discussion of Results

Considering the relative crudeness of the measurements, it is felt that a comparison with Kimzey's [5] values of 0.84 second for extinguishment of paraffin in air at 1 atm and 1.16 second in O_2 at 1/3 atm is quite satisfactory. Kimzey's photographs indicate that he was unable to eliminate convection completely. Convection currents tend to increase extinguishment time by introducing fresh oxygen. In addition, the presence of the hot ignitor wire (which cools much slower than the flame) in contact with the relatively cold paraffin may have increased the flame extinguishment time.

Kimzey's paraffin flames exhibited maximum brightness after about .44 second from ignition. Such a maximum is predicted by the theoretical model described in paragraph 2.3.2.3 and Fig. 7.

A factor that cannot be overlooked is the influence of the geometric shape of the flame on its radiative properties. Kimzey's flames were for spherical fuels. Energy loss by radiation can occur in all directions and thus may accelerate extinction.

2.3.3.5 Recommendations

These preliminary results show that information about the behavior of diffusion flames under conditions of zero-g can be obtained in the laboratory. If more quantitative results are desired, accurate measurements should be made of the flame velocity, temperature, thickness, gas composition and thermal radiation.

It is recommended that the Apollo Applications Program consider the possibility of including a number of tests with flat combustible surfaces to check the adequacy of the theoretical models proposed in this study.

2.3.4 Other Methods for Simulating Zero-G

The absence of convection currents and the generation and accumulation of partially combusted products near the burning surface are the two fundamental features of a zero-g fire. The feasibility of reproducing these features by two other methods was investigated but not carried beyond a preliminary experimental stage. Most of the study was devoted to the flat diffusion flame burner which promised more quantitative data within the available time. The other methods were:

a. The application of an electrostatic field to the flame:

A flame consists of neutral molecules, atoms and free radicals, positive and negative ions and electrons. The ion concentration of a pre-mixed flame is of the order of 10^{-5}% with the number of positive ions roughly equal to the number of electrons, the negative ions constituting only a negligible fraction of the negative charge carriers. The "ionic wind" generated when a flame is placed in an electrostatic field has been a scientific curiosity for the past three centuries. Only recently did the possibility of applying these effects to engineering advantage occur to research scientists. It is generally believed that the "ionic wind" is generated because of collisions between the relatively heavy positive ions and the neutral species when the flame is placed in an electrostatic field. These forces can distort the shape of the flame considerably[12]. If the electric field were applied in such a manner that the "ionic wind" cancels the upward motion of the flame due to convection, then the absence of gravity will be approximately simulated. Two objections have been raised concerning this approach. One is that the

electrostatic field will not cancel the convection currents in the unionized air or cold combustion gases surrounding the flame. The other is that the electrostatic field may alter the kinetics of the reactions in the flame[13]. Nakamura's experiments, however, showed that neither the number of ions nor the extent of excitation of radicals in the flame was affected by the applied field except for a physical displacement[14].

b. The second method for simulating combustion during weightlessness is to allow burning to take place along the bottom surface of the material. The hot and thus lighter combustion products will accumulate near the surface and any oxygen needed to support the combustion process will have to diffuse through this layer. This again reproduces the essential features of zero-g combustion and the theoretical model described in Section 2.2.

These two methods deserve further consideration in any future studies on the simulation of combustion during zero-gravity.

3. TEMPERATURE AND PRESSURE RISE DUE TO A FIRE IN AN ENCLOSURE

3.1 Introduction

An uncontrolled fast combustion process taking place in an unvented enclosure may result in temperatures and pressures which cannot be tolerated by the walls or contents. Regardless of whether this enclosure is a hermetically sealed electronic box, a laboratory combustion test glass jar, a space vehicle or a hyperbaric chamber, an accidental fast developing fire may result in disastrous consequences.

It is the objective of this section to consider all possible models for the burning process within an enclosure containing an excess of oxidant and to develop the equations describing the variation of temperature and pressure with time. The results predicted by these equations will then be examined in the light of the few available experimental data.

3.2 Conditions Leading to a Fire in an Enclosure

The presence of an adequate supply of fuel, oxidant (usually oxygen) and thermal energy is a prerequisite for the initiation of a fire. The ease of ignition of a fuel depends upon several factors among which are its ignition temperature, chemical composition, geometric shape and spatial distribution.

The rate of burning of solid combustible materials has been shown to increase sharply with an increase in oxygen concentration[15], and with the total pressure[16]. Certain materials that do not ignite in air burn readily as the oxygen concentration is increased[17]. In addition to changes in the flame spread rate, the ignition temperature is lowered significantly when the total pressure or the concentration of O_2 is increased [18],

while equilibrium flame temperatures in pure oxygen atmospheres are always higher than those in air, because of the absence of diluent. Furthermore, storage in pure oxygen for prolonged periods of time has an unpredictable but significant effect on the rate of burning of certain materials[15].

Thermal energy necessary to initiate a fire could come from an outside source, such as by overheating due to a surge in an electric wire, contact with a high temperature object, radiant energy from another fire, etc., or may be generated within the fuel by a slow reaction with the oxidant so that the rate of heat generation exceeds the rate of heat loss to the surroundings (auto-ignition).

Since the use of pure oxygen offers the greatest hazard in space applications, the analysis and equations below have been developed for a pure oxygen atmosphere. However, the equations can be very easily modified to account for the presence of other diluents.

3.3 Temperature and Pressure Dependence on Mass Burnt in an Adiabatic Enclosure:

Combustion in an adiabatic enclosure produces the maximum possible temperatures and pressure. The derivation below assumes complete mixing and ideal gas behavior. In the reaction

$$C_c H_h O_x + (c + \frac{h}{4} - \frac{x}{2}) O_2 \longrightarrow cCO_2 + \frac{h}{2} H_2O$$

M grams of a typical organic fuel, $C_cH_hO_x$, react with $(c + \frac{h}{4} - \frac{x}{2})$ moles of O_2 to produce $(c + \frac{h}{2})$ moles of product gases. At any time after ignition, the total number of moles present, N_{total}, will be

$$N_{total} = N_{O_2} - \frac{m}{M}(c + \frac{h}{4} - \frac{x}{2}) + \frac{m}{M}(c + \frac{h}{2})$$

$$= N_{O_2} + \frac{m}{M}(\frac{h}{4} + \frac{x}{2})$$

where M = molecular weight of $C_cH_hO_x$

m = mass of $C_cH_hO_x$ burnt by that time (g).

N_{O_2} = number of moles of oxygen initially present (g-mole).

An energy balance after time t from ignition can be written for this enclosure with no heat losses to the wall or to the contents of the enclosure. This would be approximately the case during a very fast combustion process.

$$\frac{dm}{dt} H_o = \bar{C}_p \left\{ N_{O_2} + \frac{m}{M} \left(\frac{h}{4} + \frac{x}{2}\right) \right\} \frac{dT}{dt} + \bar{C}_p \left(\frac{h}{4} + \frac{x}{2}\right) (T-T_o) \frac{1}{M} \frac{dm}{dt}$$

$$= \frac{d}{dt} \left\{ \bar{C}_p \left[N_{O_2} + \left(\frac{h}{4} + \frac{x}{2}\right) \frac{m}{M} \right] (T-T_o) \right\} \qquad (52)$$

where H_o = heat of combustion of $C_cH_hO_x$ at T_o (cal/g)

$\bar{C}_p$ = average specific heat of all gases in the enclosure (cal/g-mole ^oC)

T = temperature of the gas at time t (^oK)

T_o = initial temperature (^oK)

Integrating equation (52) gives

$$m H_o = \bar{C}_p \left\{ N_{O_2} + \left(\frac{h}{4} + \frac{x}{2}\right) \frac{m}{M} \right\} (T-T_o)$$

$$\text{or } T = \frac{m H_o}{\bar{C}_p \left\{ N_{O_2} + \frac{m}{M} \left(\frac{h}{4} + \frac{x}{2}\right) \right\}} + T_o \qquad (53)$$

Equation (53) can also be derived by taking an overall energy balance on the adiabatic enclosure.

The corresponding equation relating pressure ,P, to the total mass burnt ,m, can be derived from equation (53) and the gas laws. Assuming perfect behavior

$$P_o V = N_{O_2} R T_o \qquad (54)$$

$$P V = \left\{ N_{O_2} + \left(\frac{h}{4} + \frac{x}{2}\right) \frac{m}{M} \right\} R T \qquad (55)$$

where P_o = initial pressure of the enclosure (atm)

R = gas constant (atm cm^3/g-mole ^oK)

V = volume of enclosure (cm^3)

Combining equations (53, 54 and 55), one obtains

$$\frac{P}{P_o} = \left\{1 + \frac{m}{MN_{O_2}} \left(\frac{h}{4} + \frac{x}{2}\right)\right\} + \frac{m H_o}{\overline{C}_p N_{O_2} T_o} \tag{56}$$

For example, when 20 g of cellulose ($C_6H_{10}O_5$) is burnt adiabatically in a 125 liter chamber initially at 1 atm and 300^{o}K and containing pure oxygen, a theoretical final temperature of 2163^{o}K and a pressure of 9.33 atmospheres can be calculated. In practice, these temperatures and pressures are never achieved because of heat losses to the contents, walls and to the outside.

In order to find the variation of temperature and pressure with time, a model for burning which gives the dependence of burning rate , $\dot{m}$, on time is needed. Since

$$m = \int_o^t \dot{m}\, dt \tag{57}$$

simple substitution into equations (53 and 56) of the appropriate relationship between $\dot{m}$ and time will yield the desired equations.

3.4 Variation of Burning Rate with Time

The burning rate of a solid depends on its geometric shape and spatial distribution. Simple models for burning are postulated below with their corresponding dependence of burning rate on time. The models are also illustrated in figure 11.

a. Constant burning rate:

$$\dot{m} = k_1 \tag{58}$$

Two examples where a constant rate of burning is obtained are:

(i) A thin combustible rectangular sheet ignited along one

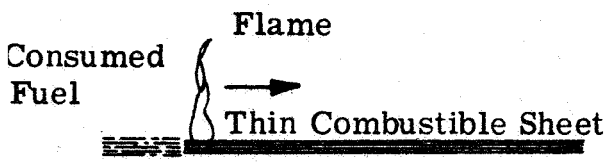

a (i)

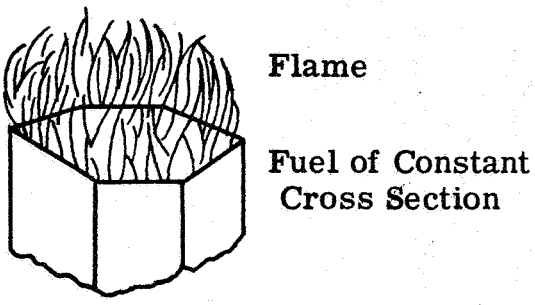

a (ii)

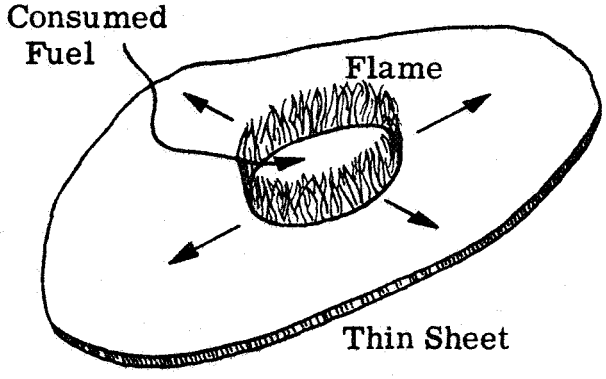

b (i)

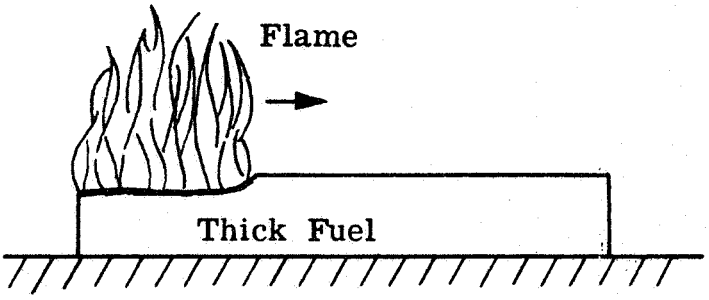

b (ii)

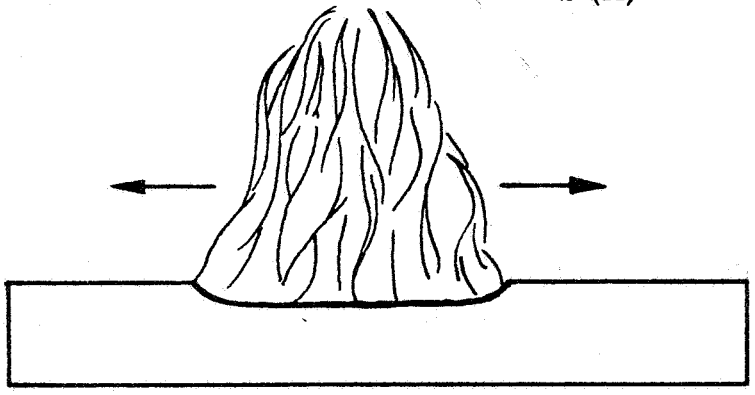

c

Fig. 11 - SIMPLE MODELS FOR BURNING

edge. The sheet is totally consumed behind the flame and the length of the flame front is always constant.

(ii) A fuel having a constant cross section burning downwards a steady state.

b. Linear dependence of burning rate on time:

$$\dot{m} = k_2 t \tag{59}$$

A linear dependence of burning rate on time is obtained in the following examples:

(i) A thin combustible sheet ignited at the center with the flame front expanding in all directions. The area between the flame and the ignition point is totally consumed.

(ii) The same as a(i) above but where the thickness of the material is large enough so that the area behind the flame continues to burn.

c. Burning rate dependent on the square of time:

$$\dot{m} = k_3 t^2 \tag{60}$$

This corresponds to combustion along the surface of a thick fuel where the flame front is expanding at a constant linear rate in all directions as in b(i) above but where the area between the flame front and the ignition point continues to burn. Equation (60) is true for turbulent flames only. (For laminar flames equation (59) is applicable).

d. Exponential dependence on time:

$$\dot{m} = k_4 e^{k_5 t} \tag{61}$$

The worst possible case for burning occurs when the fuel and oxygen are uniformly distributed and when the oxygen can gain access to all elements of the fuel at a constant predetermined rate[19].

In this case

$$\frac{dm}{dt} = k_5 m$$

$$\text{or} \qquad m = m_o e^{k_5 t} \tag{62}$$

which reduces to equation (61) above upon differentiation.

Another way of arriving at the same expression is to consider a system consisting of several fuel elements each being similar to that described under c above. A fraction of the total heat generated , α , goes into evaporating more fuel i.e.

$$\alpha \dot{Q} = \frac{dA}{dt} C_p \rho \tau (T_{vap} - T_o) \tag{63}$$

where $\dot{Q}$ = rate of heat generation (cal/s)

A = area burnt (cm^2)

$C_p \rho \tau (T_{vap} - T_o)$ = energy required per unit surface area to raise fuel temperature to vaporization (cal/cm^2)

But since $\dot{Q} \sim \dot{m}(t)$

and $\dot{m}(t) \sim A(t)$ for the model described under paragraph c above

then $A(t) = k_6 \frac{dA(t)}{dt}$

which again leads to equation (61).

A third way of arriving at the same result is to say that the rate of evaporation and eventual burning of a fuel in an adiabatic enclosure is proportional to the total heat content of the enclosure which, in turn, is dependent on the total amount of fuel burnt up to that time, i.e.

$$\frac{dm}{dt} \sim Q \sim m$$

where Q = heat content of enclosure (cal)

Regardless of the method of derivation, this model assumes that an initial small fire consumes a mass m_o by one of the other mechanisms

described in a, b or c above before it grows exponentially (i.e. at t=0, $m=m_o$). This behavior has been observed experimentally by Denison et al [20] in experiments with denim overalls burnt in oxygen atmospheres. Within 0.6 second after ignition, a flame had swept over the whole surface in the manner described by model b(i) above, after which edges of sleeves and trouser legs began to burn. After 7.5 seconds, 30% of the overalls was burning and at 11.3 seconds, the whole surface was engulfed by intense flames.

It should be pointed out that the burning rate of a mixture of combustibles having different configurations would be extremely difficult to predict from the burning rates of the individual components. The fast burning, high heat generating combustible will be a controlling factor contributing towards a general increase in the burning rates of adjacent combustibles. On the other hand, the presence of a flame retarding agent in one combustible may inhibit the rate of burning of another highly combustible element.

3.5 Comparison of Experimental Data with Theoretical Predictions

With all the experimental studies that have been performed on the flammability of materials in oxygen enriched atmospheres, very little data are available in the literature on the variation of enclosure temperature and pressure during combustion. A number of studies have been performed by Botteri[29], but the pertinent data has not been extracted from recorder charts yet. Only one of his plots of pressure vs. time is available[21] for the combustion of a stoichiometric amount of cotton in an oxygen filled chamber, 45.25 liters in volume at half an atmosphere. This plot is reproduced in figure 12.

Another source of data was the record of the Apollo 204 space cabin fire[22].

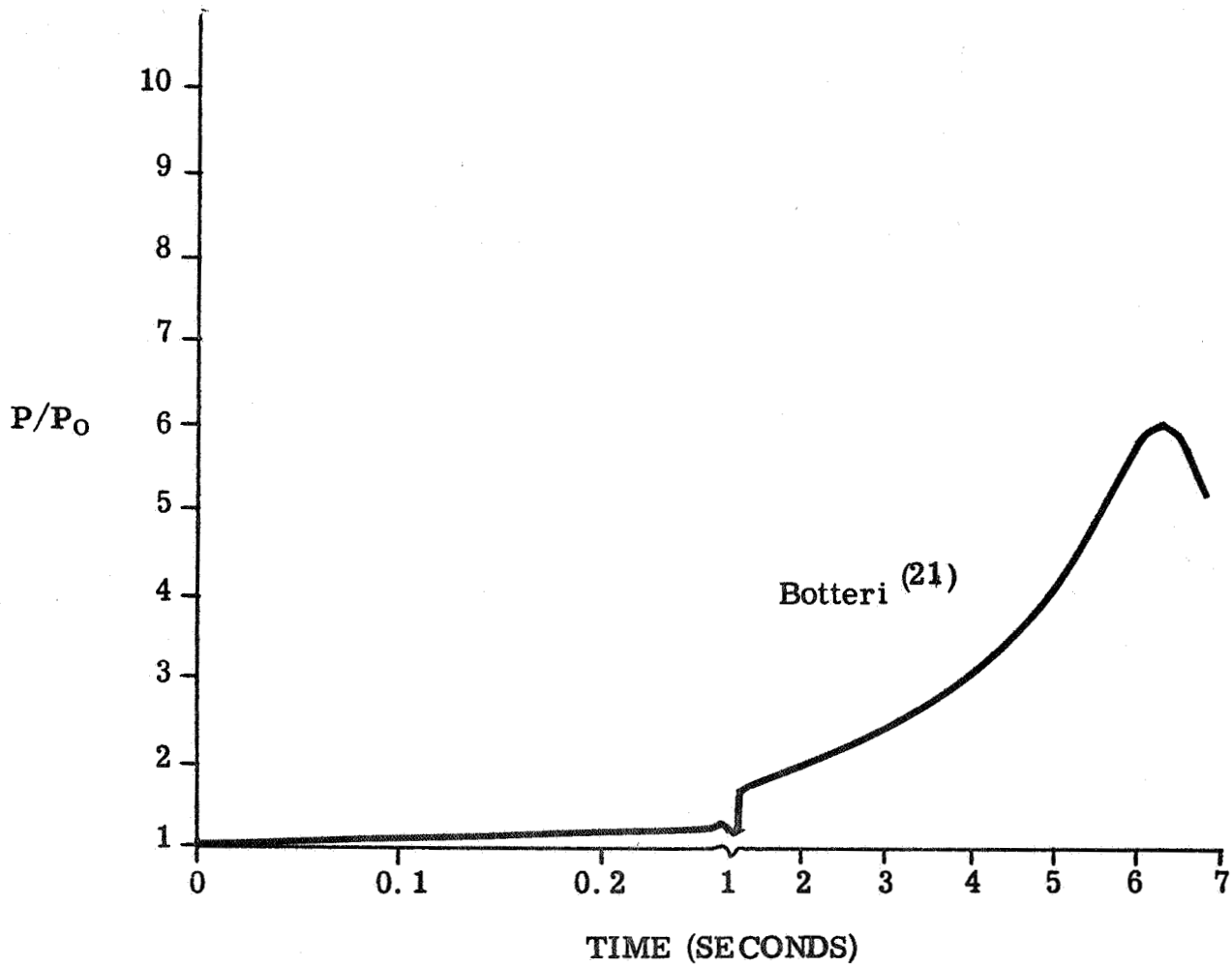

Fig. 12 Pressure profile during the combustion of cellulose in oxygen.

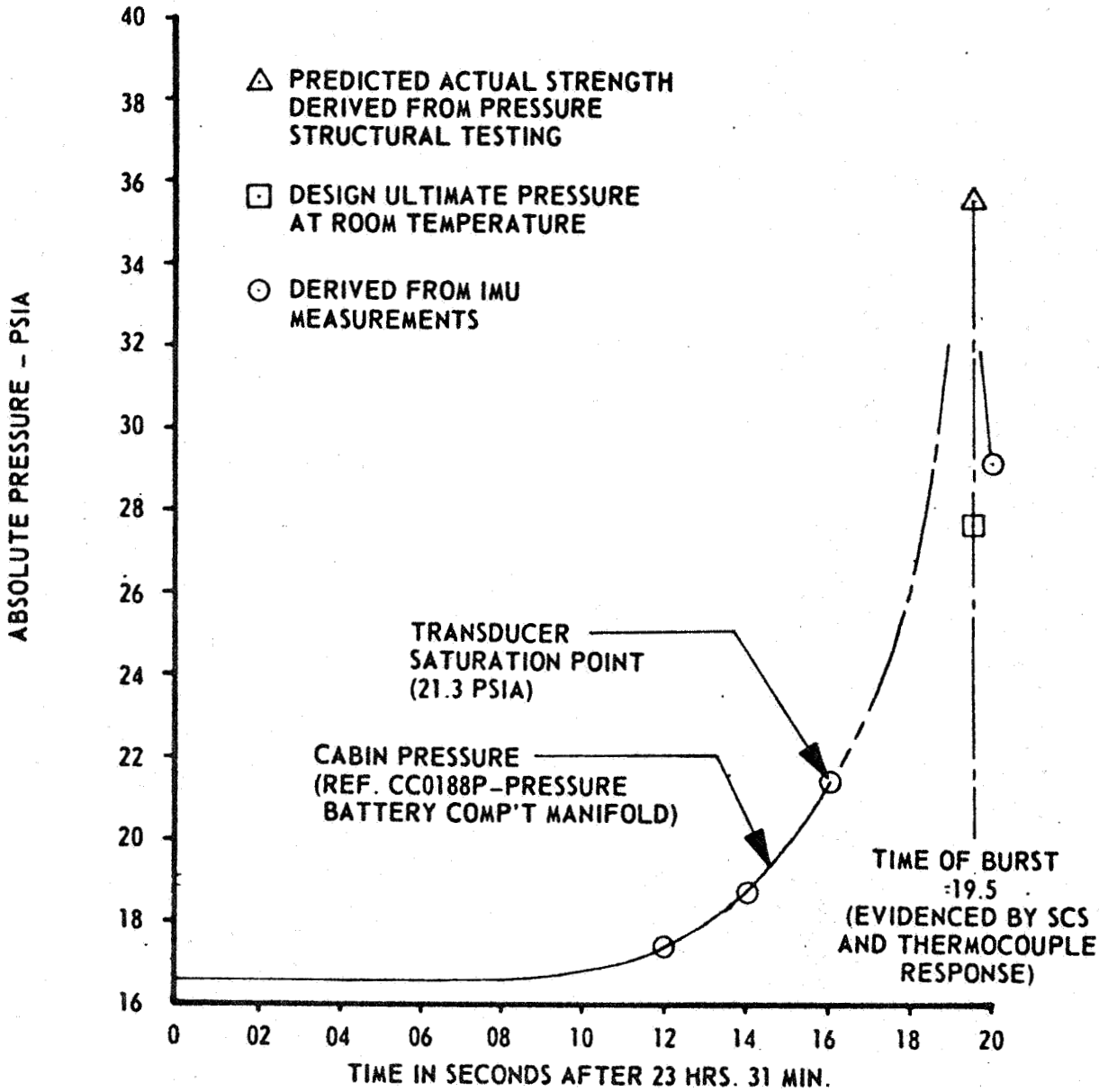

Fig. 13 Apollo 204 Cabin Pressure During the Fire(22).

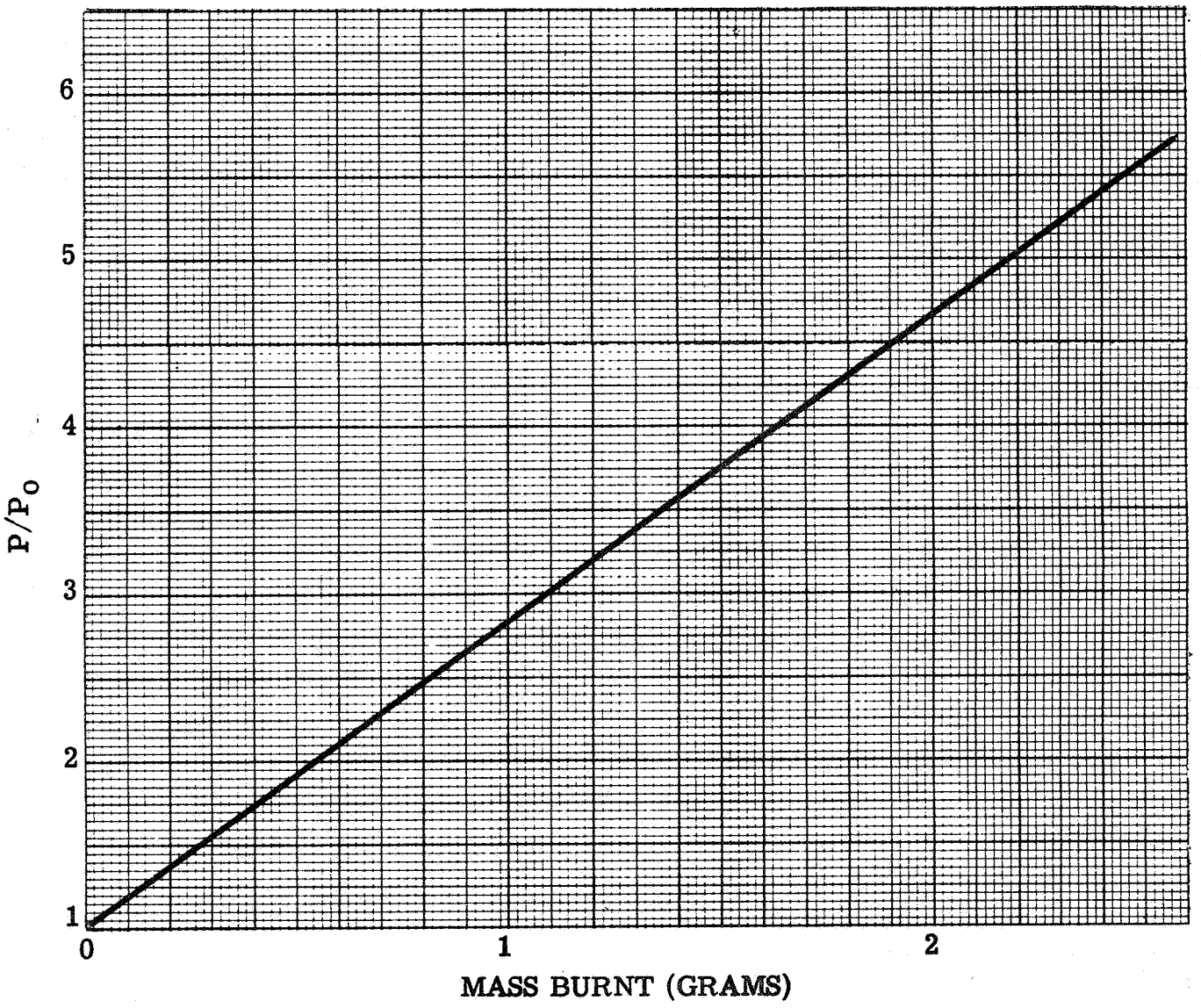

Fig.14 - Plot of P/P_0 versus mass burnt for Botteri's experiment as predicted by equation (56).

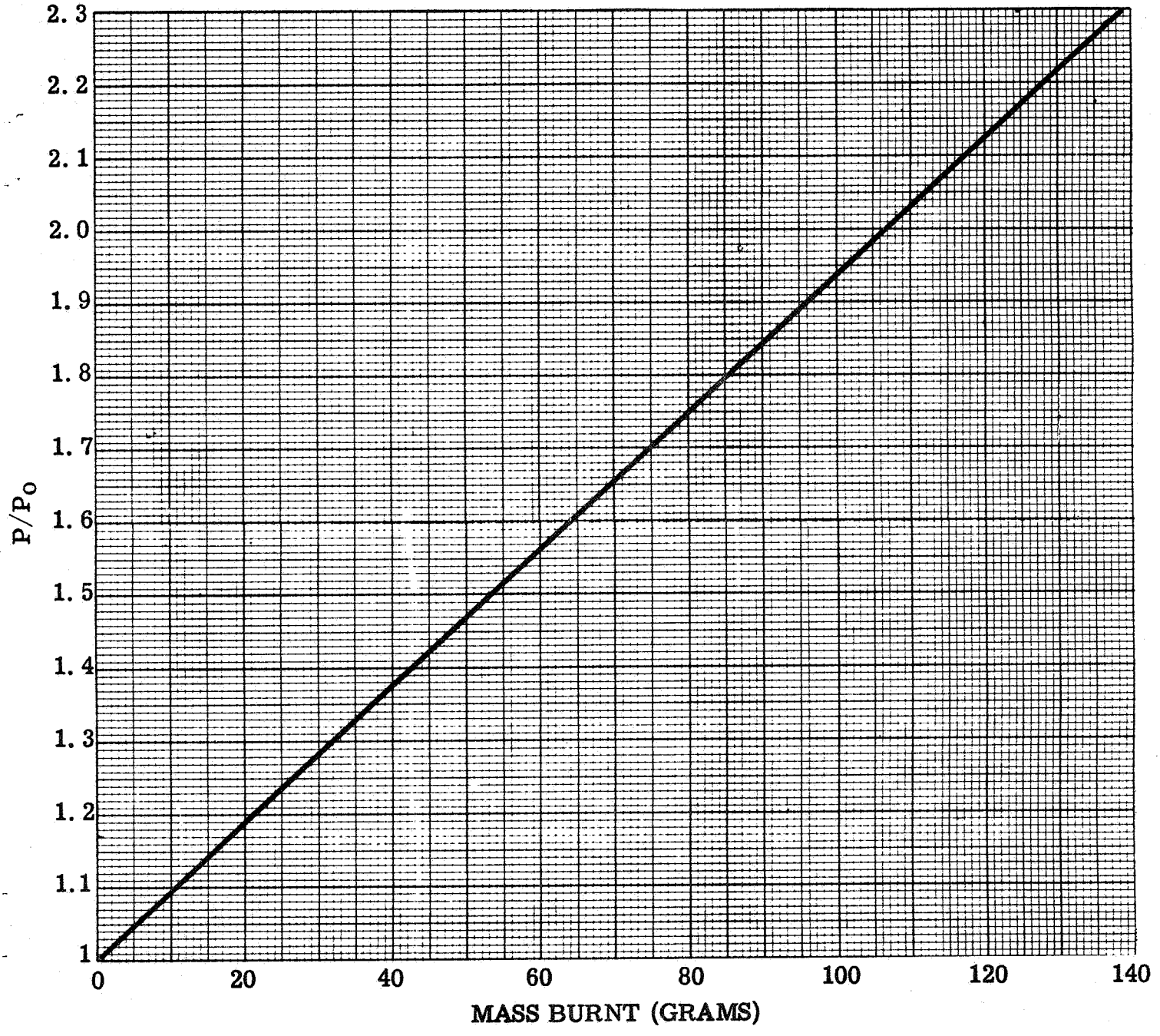

Fig.15 - Plot of P/P_0 versus mass burnt for the Apollo accident as predicted by equation (56).

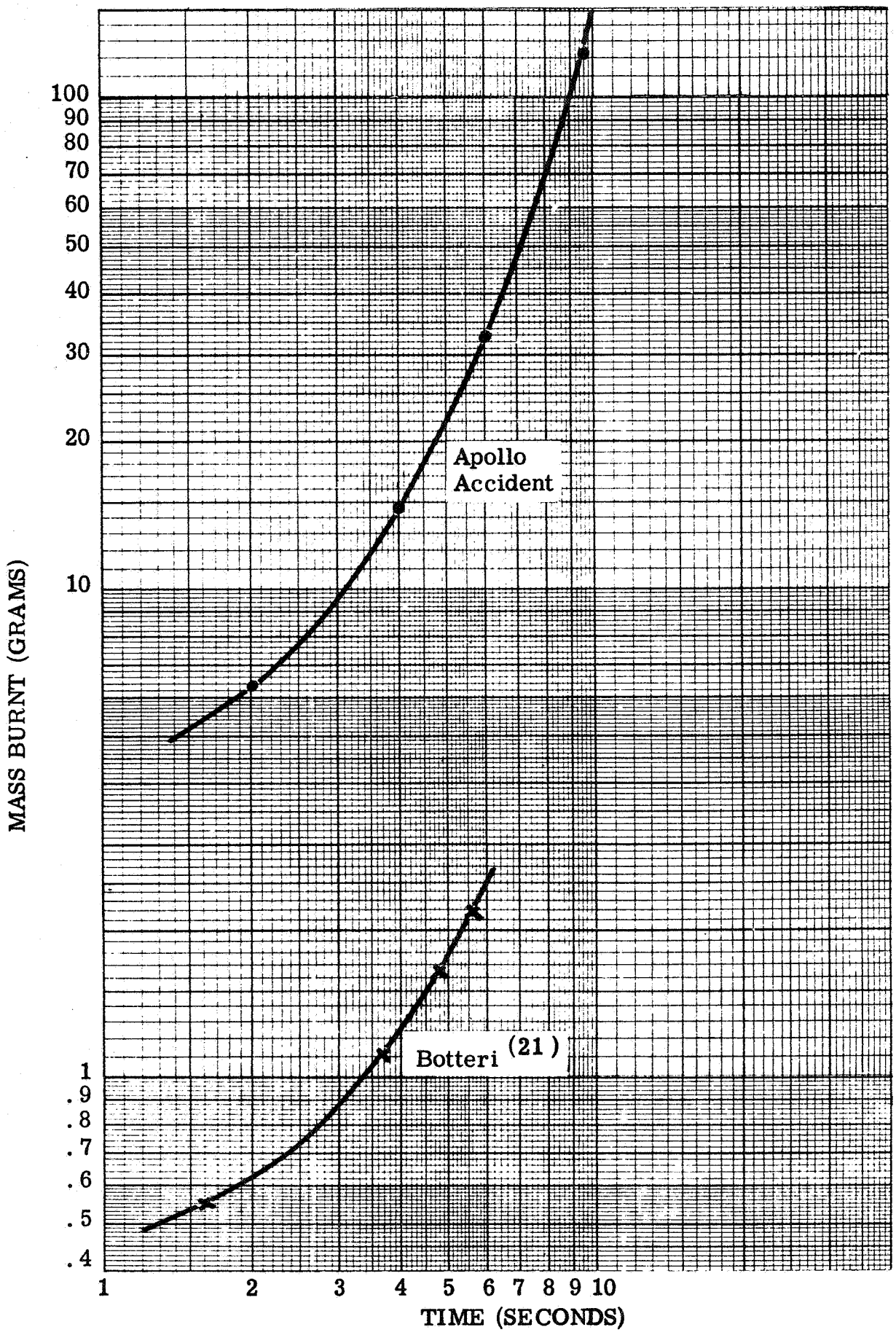

Fig. 16 - Log-log plot of mass burnt versus time for the Apollo accident and Botteri's experiment

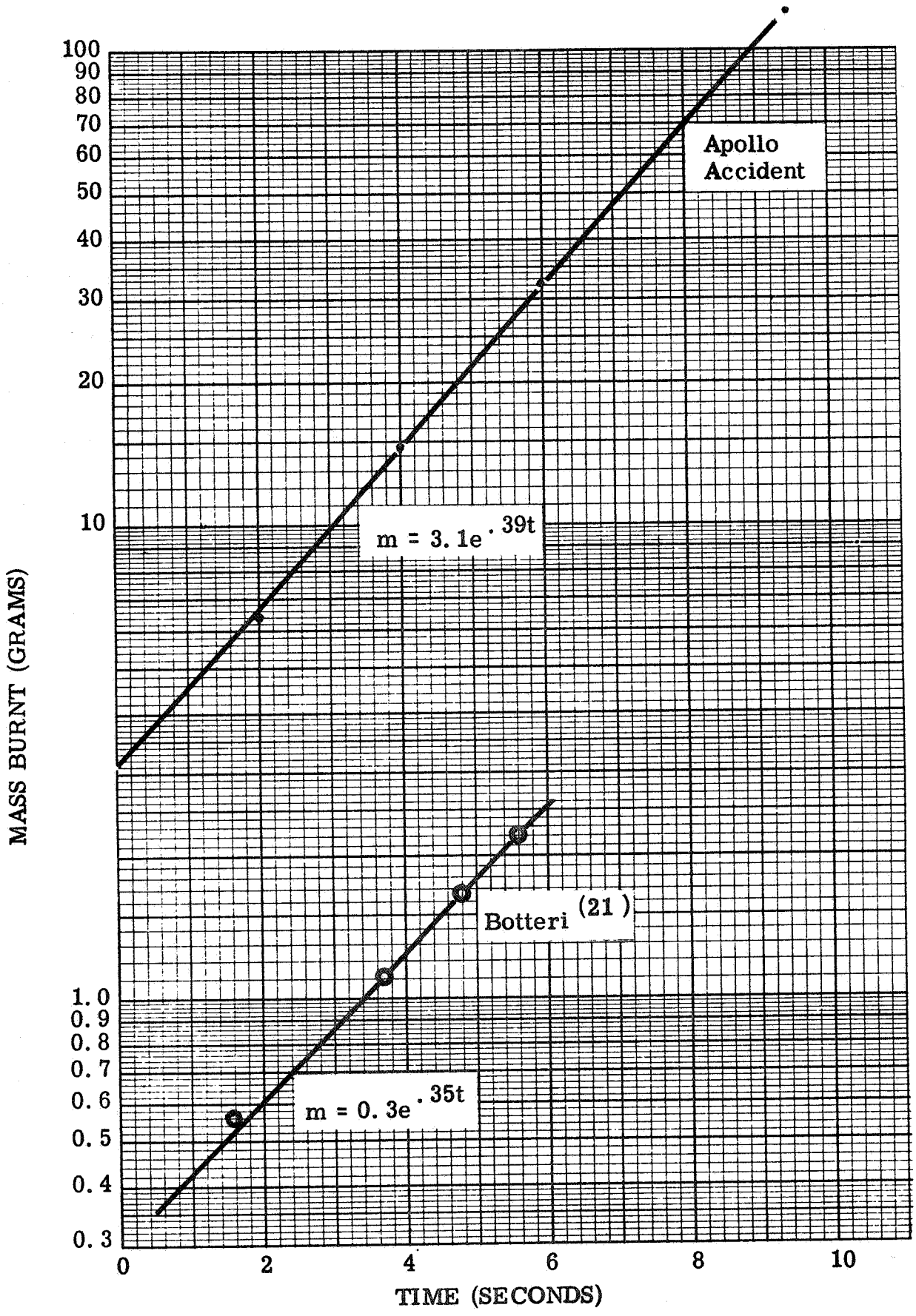

Fig. 17 - Semi-Log Plot of Mass Burnt Versus Time for the Apollo accident and Botteri's Experiment

A plot of cabin pressure versus time is reproduced in figure 13.

The relation between pressure and mass burnt as predicted by equation (56) was plotted for each case. (See figures 14 and 15). The actual time taken to reach a given pressure was read from the experimental plots (figs. 12 and 13) while the mass burnt to reach that pressure was read from figs.14 & 15. The dependence of mass burnt on time was found by plotting m vs. t on log-log and semi-log paper (figures 16 and 17). It was found that the exponential model gave an excellent fit. The equations describing this dependence were

$$\left.\begin{aligned} m &= 0.3\, e^{0.35t} \\ \dot{m} &= 0.105\, e^{0.35t} \end{aligned}\right\} \text{ Botteri} \qquad (64)$$

$$\left.\begin{aligned} m &= 3.1\, e^{0.39t} \\ \dot{m} &= 1.21\, e^{0.39t} \end{aligned}\right\} \text{ Apollo accident} \qquad (65)$$

It was interesting to note that the slopes of these two lines are roughly the same. The slope is related to the fraction of chemical energy generated within the chamber which goes into heating the fuel to its vaporization temperature as shown by the equation (63). This fraction is apparently the same in both cases. On the other hand, the value of m_o depends on the scale of the experiment and the size of the ignition source.

It should also be noted that, under the assumptions made in this derivation (adiabatic, non-condensing products, etc.), only a small mass is theoretically needed to burn exponentially in order to achieve the pressures actually reached in both systems. About 110 and 2.2 grams need to have burnt in the Apollo cabin and in Botteri's chamber respectively before the pressure reached a maximum value.

Apparently, during the initial stages of the combustion process in an oxygen enriched atmosphere, the reaction is so fast that the system does follow the assumptions made in the derivations. However, at a certain point, heat losses to the wall and contents, water vapor condensation on the cold walls and the dilution of oxygen with combustion products become significantly large, so that even though the combustible contents continue to burn, the pressure begins to drop.

The escape of gases from the Apollo vehicle due to wall failure was another major factor in reducing the pressure. Obviously, heat losses to the walls and contents and dilution of oxygen were more important factors in Botteri's small chamber than in the much larger Apollo vehicle.

3.6 Recommendations

Further work in this area is needed to verify theoretical predictions. The following factors should be investigated:

(i) Effect of configuration (see figure 11) on the temperature and pressure variation with time.

(ii) Effect of the size and shape of the enclosure on the value of m_o in equation (62).

(iii) Effect of oxygen concentration and total pressure on m_o.

4. FIRE HAZARD OF WIRE BUNDLES

4.1 Introduction

Wire bundles are widely used in spacecraft. Since ignition temperatures of materials are generally lower in oxygen atmospheres and because of the absence of convection currents in zero gravity flights, it is quite possible for the temperature within the bundle to rise to a dangerous level due to heat accumulation. The purpose of this section is to review previous work on this subject, to extend previous work to the case of a sheathed bundle and to recommend areas where further study is needed.

4.2 Previous Work

The general solution of the temperature profile in a wire bundle is not easily attainable because of the complexity of the wire distribution. In addition, there is usually a lack of information concerning current distribution in the bundle. In general, all previous work has been limited to homogeneous bundles consisting of similar wires carrying similar loads.

Jakob [23] assumed that the same amount of heat is developed in each representative volume and that the resistivity is the same throughout the bundle. The heat developed in such a body is conducted to the surface of the bundle as in a homogeneous medium the thermal conductivity of which is equivalent to that of a mixture of the materials in the bundle. But because the heat generated by the electric current is proportional to the resistance, which in turn is dependent on temperature, more heat per unit volume is produced at the warmest place inside the bundle than just below the surface where it is relatively cooler. For a non-sheathed bundle, he found that the temperature profile can be expressed by an

equation involving Bessel functions.

$$T - T_s = \frac{m}{n}\left[\frac{J_o\,(r\sqrt{n})}{J_o\,(s\sqrt{n})} - 1\right] \qquad (66)$$

where T_s = temperature at the surface (^oK)

s = radius of bundle (cm)

r = radial distance of a point in the cylinder (cm)

m,n = constants defined by the equation: $\frac{q'''}{k} = m + nT$

q''' = rate of heat energy developed per unit volume ($cal/cm^3 s$)

k = overall thermal conductivity of the bundle ($cal/cm\ ^oK$)

Using the same assumptions of Jakob, Higgins[24] solved the temperature distribution in a rectangular electric wire bundle. Higgins' solution for the temperature distribution is given by the equation:

$$T = T_s - (C'/C^2)(1 - \cos Cx \sec Ca) - (2C'/a)\sum_{i=1}^{\infty}(-1)^{i-1} \cos M_i x \cosh K_i y / (K_i^2 M_i \cosh K_i b) \qquad (67)$$

where $C^2 = q_o \alpha_o / k$

$C' = q_o (1+\alpha_o T_s)/k$

$2a,2b$ = dimensions of rectangular bundle (cm)

x, y = coordinates of point under consideration with reference to origin at center of bundle (cm)

$M_i = \pi(2i-1)/2a$, $i = 1,2,3,..$

$N_j = \pi(2j-1)/2b$, $j = 1,2,3,..$

$K_i = N^2_j - C^2$

Schach and Kidwell[25] solved the problem for the cylindrical horizontal homogeneous bundle by a numerical procedure and performed experiments to determine the heat transfer coefficient for convection and radiation from the surface, as well as to check their numerical solution.

4.3 Sheathed Wire Bundles

Most wire bundles employed in space vehicles are sheathed for protection against mechanical erosion. The analysis below considers the effect of such a sheath on the temperature distribution within the bundle.

The bundle is again assumed to consist of a large number of similar cables having a uniform load. Consider a long cylindrical wire bundle of mean thermal conductivity k_1 and radius a which is surrounded by a sheath having a thermal conductivity k_2 and outside radius b. Let θ be the difference between the temperature of any point and that of the environment, T_o

i.e. $\theta = T - T_o$

Two differential equations in cylindrical coordinates with and without heat generation govern the temperature distribution within the bundle and in the sheath, respectively.

$$\frac{d^2\theta_1}{d\,r^2} + \frac{1}{r}\frac{d\theta_1}{dr} + \frac{q'''}{k_1} = 0 \quad \text{at} \quad 0 < r < a \tag{68}$$

$$\frac{d^2\theta_2}{d\,r^2} + \frac{1}{r}\frac{d\theta_2}{dr} = 0 \quad \text{at} \quad a < r < b \tag{69}$$

Here θ_1 is the temperature difference between any point in the bundle and the environment while θ_2 is the corresponding difference for the sheath. If the resistance varies linearly with temperature, the volumetric rate of heat generation becomes a linear function of temperature, i.e.

$$q''' = q_o\,(1 + \alpha\theta) \tag{70}$$

where q_o = the heat generated per unit volume per unit time at reference temperature T_o (cal/cm^{3}s)

α = constant

Substituting equation (70) into (68) gives

$$\frac{d^2\theta_1}{dr^2} + \frac{1}{r}\frac{d\theta_1}{dr} + \frac{q_o\alpha\theta_1}{k_1} = -\frac{q_o}{k_1} \quad \text{at } 0 < r < a \tag{71}$$

Equations (71) and (69) can be easily solved to give

$$\theta_1 = A_1 J_o(\beta r) + B_1 Y_o(\beta r) - \frac{1}{\alpha} \quad \text{for } 0 < r < a \tag{72}$$

$$\theta_2 = A_2 + B_2 \ln r \quad \text{for } a < r < b \tag{73}$$

where $\beta = \frac{q_o \alpha}{k_1}$

A_1, B_1, A_2, B_2 = constants

The two constants in each equation have to be determined by the application of appropriate boundary conditions. These are:

at $r = 0$ $\quad \frac{d\theta_1}{dr} = 0$

$r = a$ $\quad \theta_1 = \theta_2$

$r = a$ $\quad k_1 \frac{d\theta_1}{dr} = k_2 \frac{d\theta_2}{dr}$

The worst case encountered in space applications is during zero gravity flight when heat losses from the surface of the bundle are due to conduction and radiation only.

Define λ by the equation $\lambda = \frac{h_c + h_r}{k_2}$

where h_c = a heat transfer coefficient for conduction (cal/cm^{2}s ^oK)

h_r = a heat fransfer coefficient for radiation (cal/cm^{2}s ^oK)

Then at $r = b$ $\quad \frac{d\theta_2}{dr} + \lambda \theta_2 = 0$

These four boundary conditions are sufficient to determine the four constants in equations (72) and (73). The final temperature profiles in the bundle and in the sheath are:

$$\theta_1 = \frac{1}{\alpha}\left[\frac{J_o(\beta r)}{J_o(\beta a) - a \frac{k_1}{k_2}\beta\left\{\frac{1}{b\lambda} + \ln\frac{b}{a}\right\} J_1(\beta a)} - 1\right] \tag{74}$$

$$\theta_2 = \frac{\frac{1}{\alpha}\left\{\frac{1}{b\lambda} + \ln\frac{b}{r}\right\}}{\frac{k_2 J_o(\beta a)}{k_1 a \beta J_1(\beta a)} - \left\{\frac{1}{b\lambda} + \ln\frac{b}{a}\right\}} \tag{75}$$

4.4 Recommendations

In practice, wire bundles consist of cables of different materials and radii and carry non-uniform loads. Thus the analytical methods described above are not applicable to this complex problem. A numerical technique such as the relaxation method will have to be employed in this case. It is recommended that the following systems which are listed in increasing order of difficulty be studied theoretically and experimentally:

(i) A bundle consisting of uniform wires but with one non-centrally located wire carrying a larger current than the remainder.

(ii) A bundle of uniform wires carrying variable currents.

(iii) A bundle of different wires each carrying the same current.

(iv) A bundle of different wires carrying different currents.

5. REFERENCES

1. M. W. Tobriner, G. von Elbe and C. K. Houston, "Quantitative Guidance for Material Control to Minimize Fire Hazards in Spacecraft", Task II Report by Atlantic Research Corp., Contract NAS 9-7057, Preliminary Draft, January 19 (1968).
2. S. Kumagai and H. Isoda, "Combustion of Fuel Droplets in a Falling Chamber", Sixth Symposium (International) on Combustion, Reinhold Publishing Co., N.Y. pp. 726-731 (1956).
3. H. Isoda and S. Kumagai, "New Aspects of Droplet Combustion", Seventh Symposium (International) on Combustion, The Combustion Institute, Pittsburgh, Pa., pp. 523-531, (1958).
4. A. L. Hall, "Observations on the Burning of a Candle at Zero Gravity" School of Av. Med. 5, (February 1964), DDC Document AD 436897.
5. J. H. Kimzey, W. R. Downs, C. H. Eldred and C. W. Norris, "Flammability in Zero-Gravity Environment", NASA Technical Report TR R-246, October, (1966).
6. M. R. Stevens, H. D. Fisher and B. P. Breen, "Investigation of Material Combustibility, Fire and Explosion Suppression in a Variety of Atmospheres", Dynamic Science, Monrovia, California, under Contract AF 22 (615)-2257, Technical Report AFAPL-TR-68-35, WPAFB, Ohio, May (1968).
7. J. H. Kimzey, "Gravity Effects on Combustion", NASA-MSC Internal Note MSC-ES-R-67-10, October (1967).
8. T. Cocran, NASA-Lewis Research Center, Cleveland, Ohio, Private Communication, June (1968).
9. H. Hottel and A. F. Sarofim, "Radiation Transfer" McGraw Hill Book Co., pp. 229-246 (1967).

10. A. M. Godridge and E. G. Hammond, "Emissivity of a Very Large Residual Fuel Oil Flame", Paper presented at the 12th Symposium (International) on Combustion held at Poitiers, France, July 14-20, 1968.

11. H. G. Wolfhard and W. G. Parker, Proceedings of the Physical Society, B, 62, 523 (1949a).

12. H. F. Calcote and R. N. Pease, "Electrical Properties of Flames - Burner Flames in Longitudinal Electric Fields", Ind. Eng. Chem. 43, 2726-2731 (1951).

13. R. J. Heinsohn and P. M. Becker, "Electrically Augmented Flames", Paper presented at the Seminar on New Developments in Combustion Engineering, Pennsylvania State University (August 4, 1967).

14. J. Nakamura, "Effect of the Electric Field upon the Spectra of Hydrocarbon Diffusion Flame", Combustion and Flame, 3, 277 (1959).

15. C. Huggett et al, "The Effects of 100% Oxygen at Reduced Pressure on the Ignitibility and Combustibility of Materials", SAM-TR-65-78, Brooks Air Force Base (Dec. 1965).

16. H. L. Turner and L. Segal, "Fire Behavior and Protection in Hyperbaric Chambers" Fire Technology, 1, No. 4, 269-277 (Nov. 1965).

17. J. E. Johnson and F. J. Woods, "Flammability in Unusual Atmospheres, Part I - Preliminary Studies of Materials in Hyperbaric Atmospheres Containing Oxygen, Nitrogen and/or Helium", Naval Research Laboratory, NLR Report 6470 (Oct. 31, 1966).

18. J. M. Kuchta, A. L. Furno, G. H. Martindill and A. C. Imhof "Ignition Temperatures and Flame Spread Rates of Materials in Oxygen-Enriched Atmospheres", Paper presented at the Eastern Section of the Combustion Institute, Carnegie-Mellon University, Pittsburgh, Pa. (Nov. 27-28, 1968).

19. R. Friedman, "A Survey of Knowledge about Idealized Fire Spread over Surfaces", Paper presented at the Eastern Section of the Combustion Institute, Carnegie-Mellon University, Pittsburgh, Pa. (Nov. 27-28, 1968).

20. D. M. Denison and W. J. Tonkins, "Further Studies Upon the Human Aspects of Fires in Artificial Gas Environments", Flying Personnel Research Committee, Ministry of Defense, RAF Institute of Aviation Medicine, Farnborough, Hants. FPRC/1270 (Sept. 1967)

21. B. P. Botteri, "Fire Protection for Oxygen-Enriched Atmosphere Application", Fire Journal, 62 No. 1, 48-55 (Jan. 1968).

22. Report of Apollo 204 Review Board - Report of Panel 5 "Origin and Propagation of Fire" Appendix D-5 Enclosure 5-8, U.S. Government Printing Office (1967).

23. M. Jakob, "Influence of Nonuniform Development of Heat Upon the Temperature Distribution in Electrical Coils and Similar Heat Sources of Simple Form" Trans. ASME, 65, 593-605 (Aug. 1943).

24. T. J. Higgins, "Formulas for Calculating the Temperature Distribution in Electrical Coils of General Rectangular Cross Section", Trans. ASME 66, 665-670 (Nov. 1944).

25. M. Schach and R. E. Kidwell, Jr., "Continuous Current and Temperature Rise in Bundled Cables for Aircraft", AIEE Trans. 71 Part II, 376-384 (Jan. 1953).